Journal of Building Engineering 70 (2023) 106316

Contents lists available at ScienceDirect

Journal of Building Engineering

journal homepage: www.elsevier.com/locate/jobe

# Seismic capacity and performance of code-conforming single-story RC precast buildings considering multiple limit states and damage criteria

Gennaro Magliulo [a,b,*], Danilo D'Angela [a], Valeria Piccolo [c], Chiara Di Salvatore [a], Nicola Caterino [c,d]

[a] University of Naples Federico II, Department of Structures for Engineering and Architecture, Via Claudio 21, 80125, Naples, Italy
[b] Construction Technologies Institute, National Research Council, Via Claudio 21, 80125, Naples, Italy
[c] University of Parthenope, Department of Engineering, Centro Direzionale di Napoli, Isola C4, 80143, Naples, Italy
[d] Construction Technologies Institute, National Research Council, San Giuliano Milanese, Milan, Italy

ARTICLE INFO

*Keywords:*
Precast building
Seismic assessment
Serviceability
Collapse
Capacity margin ratio
Reliability index

ABSTRACT

The seismic capacity and performance of code-conforming precast buildings is assessed in the study. The case study consists in single-story precast buildings designed according to Italian building code considering low to high seismicity sites and varying both geometry layout and soil conditions. The seismic behavior of the buildings is assessed through multiple-stripe analyses performed through nonlinear three-dimensional modeling. Fragility of the buildings is computed by considering several methods, and performance evaluation is based on capacity margin ratios, failure probabilities, and reliability indexes. Damage limitation, life safety prevention, and near collapse prevention performance levels are considered by accounting for multiple damage criteria and damage states, including both local and global approaches and both ductile and brittle failure of beam-to-column connections.

The paper provides guidance for implementation of seismic capacity and performance evaluation of precast buildings according to latest advances, considering both European and US approaches. The study proves that the current code prescriptions might not supply adequate seismic performance, especially in the case of more critical soil conditions (i.e., C soil type compared to A soil type). A relatively critical performance was observed for damage limitation and life safety prevention performance levels, whereas collapse performance of the buildings was adequate. The extremely critical condition associated with brittle failure of the beam-to-column connection was also confirmed. The study stresses the need for an enhancement of current design requirements and highlights the need for further investigation into the adequacy of seismic performance of precast buildings and reliability of related code-conforming design.

## 1. Introduction

The seismic vulnerability of Italian and European single-story RC precast buildings was highlighted by several post-earthquake surveys and literature studies [1–5]. These buildings typically host industrial facilities and retain economic activities that are of

* Corresponding author. University of Naples Federico II, Department of Structures for Engineering and Architecture, Via Claudio 21, 80125, Naples, Italy.
*E-mail address:* gmagliul@unina.it (G. Magliulo).

https://doi.org/10.1016/j.jobe.2023.106316
Received 2 November 2022; Received in revised form 21 February 2023; Accepted 14 March 2023
Available online 21 March 2023
2352-7102/© 2023 The Authors. Published by Elsevier Ltd. This is an open access article under the CC BY-NC-ND license (http://creativecommons.org/licenses/by-nc-nd/4.0/).

paramount interest for national and international contexts. Due to economic, efficiency, and practice advantages, single-story precast buildings are quite spread over the Italian, Mediterranean, and European territory, and their geometrical and structural features are quite similar over different contexts and tend to follow standard layouts and details. Despite the significant improvement in both design and assessment methodologies and code provisions achieved in the last decade, single-story precast buildings are still potentially extremely critical (e.g. Refs. [6–9]). For example, the code provisions might be inadequate in addressing the safety regarding beam-to-column [10,11] and cladding-to-structure connections (e.g. Refs. [12,13]). In many cases, the design process does not result in an efficient conception and realization of the buildings, implementing uneconomic solutions (e.g. Ref. [14]). The implicit risk associated with code-conforming buildings is not necessarily stable or consistent, and, in some cases, this critically varies among different case studies and applications (e.g. Refs. [15,16]).

A significant part of the literature studies addressing the seismic performance of precast buildings focused on non-conforming buildings (e.g. Refs. [17–21]). The studies that investigated the seismic behavior of code-conforming buildings mostly focused on collapse assessment and often did not account for reliable and robust capacity criteria. For example, the failure of the beam-to-column connections was rarely considered as a collapse capacity criterion, and when it was, some failure mechanisms were neglected. The seismic assessment was often aimed at (a) developing reliable modeling approaches and methods, (b) characterizing the dynamic response of the buildings and, (c) in some cases, assessing the (collapse) fragility. The seismic capacities of the investigated buildings were often evaluated considering peculiar case study applications (e.g., site conditions and building geometries) or relatively limited size record sets. The influence of the estimation methodology was not covered by previous studies. When the collapse capacities (e.g., fragilities) were estimated, unique capacity criteria, sometimes not necessarily adherent to the actual damage mechanisms, were considered, and several sensitive alternative damage conditions were not investigated. Furthermore, despite the significant number of available methods for the fragility assessment, the literature studies often estimated the fragility only considering a single method. The (collapse) capacity margins and reliability indexes, which represent the key parameters for the performance evaluation according to the latest methodologies [22], were rarely estimated, especially over Europe. In many studies, the concept of PBEE is referred to numerical analysis and seismic capacity estimation (e.g., fragility), neglecting the performance evaluation, which should represent the final outcome of the seismic assessment and the keystone of the PBEE approach. Therefore, the knowledge about the seismic performance of precast buildings is still relatively limited regarding the abovementioned aspects, despite the significant effort that the researchers invested in the last few decades.

The present study aims at covering the identified research gap and provides both methodology and quantitative results related to the evaluation of the seismic capacity and performance of (code-conforming) single-story RC precast buildings. Multiple stripe analyses (MSAs) are performed considering (a) low to high seismicity sites (in Italy), (b) different soil conditions, and (c) different representative building geometries. The selection of the case studies and the implementation of the numerical models/analyses was carried out in the framework of the Italian National project DPC-ReLUIS RINTC [16,23–25]. Damage limit state (DLS), life safety limit state (LSLS), and near collapse limit state (NCLS) were considered as limit states (LSs), favoring the use of multiple damage criteria for the derivation of the damage states (DSs). The seismic capacity is evaluated by means of the fragility assessment and considering multiple robust methodologies. The seismic performance is evaluated by estimating the capacity margin ratios, failure probabilities, and reliability indexes.

## 2. Case study and design process

The case study buildings are single-story precast industrial buildings designed according to the Italian building code (NTC) 2008 [26], similar to Eurocodes [27,28]. It is worth specifying that the Italian code was updated in 2018 [29], without any significant changes in the design of RC precast buildings. Thus, the herein provided study can be considered valid for new structures in all respects. The plan and elevation views of the building archetype are depicted in Fig. 1a and b, respectively. In particular, short-span (SS) and long-span (LS) building geometries were considered by varying the transversal (X direction) and longitudinal (Z direction) span lengths, $L_1$ and $L_2$, respectively. SS (LS) geometry building had $L_1$ and $L_2$ equal to 15.0 and 6.0 m (20.0 and 8.0 m), respectively, whereas $H$ and $H_1$ were equal to 9.0 and 7.5 m, respectively, for both geometries. The case study geometries are representative of typical configurations of RC precast industrial buildings, especially over Italy and Europe. In particular, the considered case study

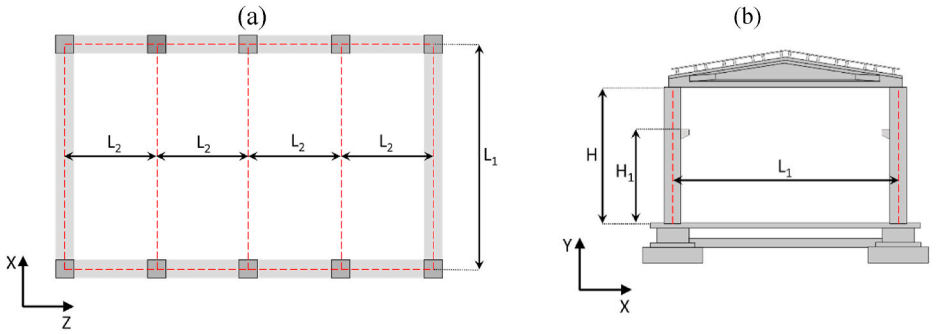


**Fig. 1.** (a) Plan and (b) elevation view of the building archetype.

layout and geometries were defined in the framework of DPC-ReLUIS RINTC project, funded by the Italian Department for Civil Protection, and aimed at the assessment of implicit seismic risk of code-conforming structures [23,24,30].

The foundations consist of socket plinths connected by RC beams along both horizontal directions. The columns have square cross-section, and they are fixed within the socket foundations. The transversal beams are prestressed and have variable cross-section width and height, with a 10% slope in the vertical plane; the longitudinal beams have a U-shaped cross-section. The beam ends are supported by the columns and the beams are fastened to the columns by dowel connections. The roof system is formed by π-shaped elements connected to the transversal beams and joined by a cast in situ concrete slab (5 cm thick); accordingly, the roof can be considered to be a rigid diaphragm. The cladding system consists of vertical precast panels (weight equal to 4 $kN/m^2$); the panels along the longitudinal (transversal) direction are fastened to longitudinal (transversal) beams. The columns present an internal corbel that bears the runway beams (HEA400 steel beams) that support the crane system.

The buildings were designed considering low-to-high seismicity sites, i.e., Milan (MI), Naples (NA), and L'Aquila (AQ), corresponding to latitude 45.465, 40.854, 42.349 and longitude 9.186, 14.268, 13.399, respectively. Soil types A and C were considered for each site, which correspond to an average velocity of the shear waves (in the upper 30 m) larger than 800 m/s and ranging within 180 and 360 m/s, respectively. The choice of such soil types is representative of the considered sites (please, see RINTC project [24,30,31]). The design was performed according to DLS and LSLS, which correspond to a return period $T_R$ equal to 50 and 475 years (probability of exceedance in 50 years ($P_{50}$) equal to 63% and 10%), respectively, for ordinary buildings with nominal life of 50 years and use class II, as in this case. The design accelerations at the bedrock ($a_g$) associated with MI, NA, and AQ sites were equal to 0.024, 0.060, and 0.104 g, respectively, for DLS, and to 0.050, 0.168, and 0.261 g, respectively, for LSLS. A medium ductility class (CDB in Italian) was assumed, corresponding to a behavior factor equal to 2.5. Concrete C45/55 and steel B450C, with a nominal yielding strength equal to 450 $N/mm^2$, were considered as materials.

The horizontal elements (beams and π-shaped elements) were designed only for vertical loads, whereas the columns were designed considering both vertical and horizontal actions. The capacity of the beam-to-column dowel connections was evaluated according to CNR 10025/84 [32], whereas the seismic demand was computed according to NTC 2008 [26]. The detailed description of the design process can be found in Ref. [33], whereas main structural details and fundamental periods of the analyzed buildings ($T_1$) are reported in Appendix A.

## 3. Methodology

### 3.1. Performance levels, limit states, damage states, and capacity criteria

According to the latest advances in structural engineering, the expected building performance is typically assessed considering standard discrete performance levels (PLs). The technical definition of PLs is based on acceptable ranges of strength and deformation attained by both structural and nonstructural members, correlated with probable levels of damage, casualties, post-earthquake occupancy, and repairs [34]. PLs are associated with seismic demand levels (e.g., according to the seismic design regulation provisions) and defined limit states (LSs). Three PLs are considered in this study: damage control or limitation PL, life safety prevention PL, and near collapse prevention PL; they are associated with DLS, LSLS, and NCLS, respectively. The seismic demand associated with the investigated LSs was derived according to NTC 2018 [29], considering the seismic design hazard parameters associated with the investigated sites [35]. In particular, the elastic acceleration response spectra were evaluated for all site and soil type conditions considering 5% damping and assuming the fundamental building period $T_1$ equal to 2.0 for all buildings (the estimated building periods $T_1$ are reported in the Appendix). LS evaluation is carried out according to the definition of consistent damage states (DSs). A DS can be defined as a quantitative condition associated with the achievement of a conventional level of damage. The general criterion for the occurrence of DS is defined in Equation (1), where $EDP_{DS}$ is the specific EDP associated with DS, and $EDP_{DS,c}$ is the EDP capacity threshold associated with DS, correlated to a DS capacity criterion.

$$EDP_{DS} \geq EDP_{DS,c} \tag{1}$$

Multiple local and global low damage to collapse DSs were considered in this study, accounting for EDPs that are relevant to the applications. In particular, the following parameters were assumed as EDPs: interstory drift ratio IDR, member end chord rotation θ, shear force acting in the beam-to-column connection system $V_{bc}$, and roof drift ratio RDR. As a matter of fact, the selection of the damage criterion can significantly condition the seismic performance assessment and the structural reliability of structures (e.g., RC structures [36]). $DS_{IDR,NSD}$ (NonStructural Damage) and $DS_{\theta y}$ were considered as low to moderate damage levels, which would correspond to building functioning interruption and repair interventions. These DSs (especially DS $_{IDR,NSD}$) are consistent with DLS defined by Eurocode 8 [27]. In particular, $DS_{IDR,NSD}$ is associated with moderate to severe damage of nonstructural systems/elements. IDR was assumed as an $EDP_{DS}$ for $DS_{IDR,NSD}$. The nonstructural elements of the case study buildings consist in the cladding system, and the earliest moderate to severe nonstructural damage occurrences are likely to involve the in-plane direction of the claddings, affecting the panel-to-structure connections, as several research studies found [12,37]. Such damage mechanisms are particularly sensitive to IDR. In quantitative terms, $DS_{IDR,NSD}$ would reasonably be correlated to the earliest of the following occurrences in each horizontal direction: (a) minor damage spread over at least 50% of the main nonstructural elements/components and (b) severe damage occurring in at least a single nonstructural element/component (without life safety threats). It is worth specifying that such assumptions have already been adopted in Refs. [31,33]. With regard to the case study buildings, the damage of the cladding system is expected to be relatively homogeneous in all claddings for each horizontal direction. The lowest panel-to-structure connection capacity corresponds to the hammer-head strap connection capacity, which can consistently be assumed in terms of displacements and expressed as an IDR. Therefore, $IDR_{NSD}$ was assumed as an $EDP_{DS,c}$ for $DS_{IDR,NSD}$, and this reported in Equation (2), which corresponds

to the mean experimental displacement capacity of the hammer-head strap connections [12] divided by the height of the building. This value also coincides with the damage limitation requirements recommended by the Eurocode 8 [27] for cases in which the nonstructural system is not expected to affect the structural deformations, which corresponds to the case study panel-to-structure connections.

$$IDR_{NSD} = 0.01 \tag{2}$$

$DS_{\theta y}$ defines the attainment of the yielding condition in terms of member end chord rotation θ ($EDP_{DS}$), which in the present case corresponds to the column base chord rotation. $\theta_y$ was considered as an $EDP_{DS,c}$ for $DS_{\theta y}$, and this was defined according to the formulation developed by Fardis and Biskinis [38] and corroborated by Fischinger et al. [39] for columns with high shear span. $\theta_y$ is reported in Equation (3), where $\varphi_y$ is the yielding curvature, $L_s$ is the shear span, $a_{sl}$ is a zero-one variable related to the slip of the longitudinal bars from their anchorage, $\varepsilon_y$ is the yield strain of the tension reinforcement, (d − d') is the distance between the tension and compression reinforcement, $d_b$ is the diameter of the tension reinforcement, $f_y$ is the yielding strength of the tension reinforcement, and $f_c$ is the compression strength of the concrete.

$$\theta_y = \varphi_y \cdot \frac{L_s}{3} + 0.00275 + a_{sl} \cdot \frac{\varepsilon_y}{d - d'} \frac{0.2 \cdot d_b \cdot f_y}{\sqrt{f_c}} \tag{3}$$

$DS_{IDR,SD}$, $DS_{IDR,4\%}$, $DS_{\theta u}$, $DS_{Vbc,d}$, $DS_{Vbc,b}$, and $DS_{RDRu}$ were considered as significant to sidesway-like collapse damage levels. $DS_{IDR,SD}$ is associated with major damage of the structure according to the provisions of the draft of the new Eurocode [40]. In particular, Equation (4) reports the IDR limit associated with this latter DS ($IDR_{SD}$).

$$IDR_{SD} = 0.02 \tag{4}$$

In order to investigate the building performance associated with IDR levels higher than $IDR_{SD}$, a further IDR-based DS ($DS_{IDR,4\%}$) was considered in this work, and Equation (5) shows the related IDR limit ($IDR_{4\%}$).

$$IDR_{4\%} = 0.04 \tag{5}$$

$DS_{\theta u}$ is associated with the ultimate conditions in terms of member end chord rotation θ ($EDP_{DS}$), which corresponds to column base chord rotation. $\theta_{u,80\%}$ was considered as an $EDP_{DS,c}$ for $DS_{\theta u}$, and this was defined by the chord rotation associated with a drop of 20% of the moment strength from the capping moment value over the softening branch. This condition was often considered in the literature for the identification of the local rotational capacity related to ultimate conditions (e.g. Ref. [36]). The formulation of $\theta_{u,80\%}$ assumed in this work follows the definition of the moment-rotation backbone by Haselton and Deierlein [41] and Haselton et al. [42] and assessed with regard to precast buildings by Fischinger et al. [39]. The formulation of $\theta_{u,80\%}$ is reported in Equation (6), where $\theta_c$ and $\theta_{pc}$ are the capping and post-capping chord rotations defined in Equations (7) and (8), respectively. In particular, $\nu$ is the normalized axial load, $\rho_{sh}$ is the transverse reinforcement ratio, and $\rho_l$ is the longitudinal reinforcement ratio.

$$\theta_{u,80\%} = \theta_c + 0.2 \cdot \Delta\theta_{pc} \tag{6}$$

$$\theta_c = 0.12 \cdot (1 + 0.4\, a_{sl}) \cdot (0.2)^{\nu} \cdot (0.02 + 40\, \rho_{sh})^{0.52} \cdot (0.56)^{0.01 f_c'} \cdot (2.37)^{10 \cdot \rho_l} \tag{7}$$

$$\theta_{pc} = 0.76 \cdot (0.031)^{\nu} \cdot (0.02 + 40 \cdot \rho_{sh})^{1.02} \leq 0.10 \tag{8}$$

$DS_{Vbc,d}$ and $DS_{Vbc,b}$ are associated with the failure of the beam-to-column connection, considering ductile and brittle failure types, respectively. The ductile failure of the connection is caused by yielding of the dowels and crushing of the surrounding concrete (mode I failure, according to Vintzēleou and Tassios [43]); the brittle failure is associated with concrete cracking and cover spalling (mode II [43])). In particular, the occurring of a ductile or brittle failure typically depends on the ratio $c/\varphi_D$, where c is the dowel concrete cover and $\varphi_D$ is the nominal diameter of the dowel. A larger (smaller) ratio, e.g., equal to 8 (4), is associated with a ductile (brittle) failure [43]. Despite the brittle failure is likely to be prevented by current design prescriptions (e.g., geometrical details), there could be cases in which the beam-to-column connections may exhibit a brittle failure (e.g., inadequate fulfillment of the design prescriptions or inadequate code prescriptions) (e.g. Refs. [10,44]). Accordingly, it is meaningful to also account for this latter failure mode, especially for comparison purposes. The following formulations were considered for the estimation of the ductile failure capacity: CNR 10025/84 [32], SAFECAST [45,46], EOTA (monotonic and cyclic) [47,48], and Vintzēleou and Tassios [43,49] (monotonic), whereas SAFECAST [45,46], EOTA (monotonic and cyclic) [47,48], Vintzēleou and Tassios [43,49], and Zoubek et al. [44] formulations were used for the brittle failure capacity. These are summarized in Table 1 (the extended formulations are not reported for the sake of brevity). Regarding the brittle failure criteria, only the case of column-side failure was taken into account since the presence of the confinement action due to the presence of the fork should prevent the beam-side failure [10].

**Table 1**
Formulations considered for the estimation of the ductile and brittle failure capacity of the beam-to-column connection.

| failure type | ductile | | | | | brittle | | | | |
|---|---|---|---|---|---|---|---|---|---|---|
| notation | $V_{R,d,CNR}$ | $V_{R,d,SC}$ | $V_{R,d,EOTA,m}$ | $V_{R,d,EOTA,c}$ | $V_{R,d,VT,m}$ | $V_{R,b,SC}$ | $V_{R,b,EOTA,m}$ | $V_{R,b,EOTA,c}$ | $V_{R,b,VT}$ | $V_{R,b,ZFI}$ |
| reference | [32] | [45,46] | [47,48] | [47,48] | [43,49] | [45,46] | [47,48] | [47,48] | [43,49] | [44] |

The shear force acting in the beam-to-column connection $V_{bc}$ was assumed as an $EDP_{DS}$, and $V_{u,bc,d}$ and $V_{u,bc,b}$ were considered as an $EDP_{DS,c}$ for $DS_{Vbc,d}$ and $DS_{Vbc,b}$, respectively. In particular, $V_{u,bc,d}$ (Equation (9)) and $V_{u,bc,b}$ (Equation (10)) are the minimum capacities associated with ductile and brittle failure formulations. For further details, please refer to the work by Cimmino et al. [10].

$$V_{u,bc,d} = \min\left\{V_{R,d,CNR}, V_{R,d,SC}, V_{R,d,EOTA,m}, V_{R,d,EOTA,c}, V_{R,d,VT,m}\right\} \tag{9}$$

$$V_{u,bc,b} = \min\left\{V_{R,b,SC}, V_{R,b,EOTA,m}, V_{R,b,EOTA,c}, V_{R,b,VT}, V_{R,b,ZFI}\right\} \tag{10}$$

$DS_{RDRu}$ is associated with a significant inelastic degradation of the building, associated with a relatively reduced margin regarding the collapse for horizontal actions. RDR and $RDR_u$ where assumed as $EDP_{DS}$ and $EDP_{DS,c}$, respectively. In particular, $RDR_u$ defines the roof drift ratio associated with a drop of 50% of the shear strength from the capping shear value over the softening branch considering the pushover curve associated with the nonlinear static analysis of the building. This condition was recently referred to in the literature to identify the ultimate conditions of various typologies of buildings (RINTC project [31,33,50]). In particular, $RDR_u$ criterion can be representative of a global mechanism and sidesway-like collapse condition, considering the strength reduction occurring throughout hysteretic cycles during seismic excitation. $RDR_u$ is defined in Equation (11) considering the pushover (PO) curve $V_h$(RDR), where $RDR_c$ is the capping RDR.

$$RDR_u = RDR > RDR_c : V_h(RDR) = 0.5\ \max(V_h) \tag{11}$$

Table 2 reports a summary of the investigated DSs and related capacity criteria/formulations. $DS_{IDR,NSD}$ and $DS_{\theta y}$ are compliant with limited damage conditions; in particular, they are associated with damage limitation PL and DLS. $DS_{IDR,SD}$ to $DS_{Vbc,b}$ are related to severe damage condition, corresponding to which the building still retains a safety margin regarding the collapse under horizontal actions; they are associated with life safety prevention PL and LSLS. $DS_{RDRu}$ is related to extremely severe damage conditions, relatively close to the collapse occurring; $DS_{RDRu}$ is associated with near collapse prevention PL and NCLS.

Table 3 reports the seismic demand spectral acceleration $Sa(T_1)$ related to AQ, associated with the respective LSs and DSs. In particular, three seismic demand conditions were considered for NCLS: $NCLS_1$, i.e., the Italian NCLS provisions ($T_R$ equal 975 years) [29], $NCLS_2$, i.e., a more severe NCLS condition often considered in codes and literature ($T_R$ equal 2745 years) (e.g., Eurocode [27] and US codes [51]), and $NCLS_3$, i.e., 1.5 times the LSLS demand (i.e., design earthquake (DE) demand as two-thirds maximum considered earthquake (MCE) demand, according to US building codes [22,52]).

### 3.2. Inelastic modeling

Three-dimensional structural models of the designed buildings were implemented in OpenSees [53]. The models included columns and longitudinal/transversal beams. The base columns were fixed at their bases to simulate the socket foundation conditions, and the horizontal elements were pinned to the columns's top to implement the dowel connections. The geometrical eccentricities of the structural elements were taken into account by rigid links. The roof elements were not included within the model, and a rigid diaphragm behavior was assigned to the horizontal members to simulate 5-cm deep cast-in-situ concrete slab. The claddings were not explicitly modeled, and their presence was only considered in terms of masses and applied loads. As a matter of fact, the considered panel-to-structure connections (i.e., hammer-head strap connections) typically exhibit the failure corresponding to relatively low seismic intensities. Therefore, the presence of the cladding system could affect the global elastic response and would have a negligible influence on the inelastic to collapse response (e.g. Refs. [13,54]). Further comments on this can be found in Ref. [10].

The horizontal elements were assumed to be elastic linear, and the behavior of the columns was modeled according to the lumped plasticity approach (i.e., phenomenological model) [31,55]. In particular, the moment-rotation response of the columns followed the peak-oriented hysteretic degradation model developed by Ibarra and Krawinkler [56] and Ibarra et al. [57] (i.e., *IMK model*). Each column member was modeled by a two-element series defined over the base, internal, and top nodes; the base and internal nodes had the same coordinates. The series system consisted of (a) an elastic-plastic rotational (dimensionless) spring and (b) an elastic (longitudinal) element. A schematic of the column series system is shown in Fig. 2. a. The spring was defined between the base and internal nodes by a *zeroLength* element, where the uniaxialMaterial ModIMKPeakOriented response was assigned [53,58]. The elastic element was modeled by *elasticBeamColumn element*. The definition of the IMK model is based on (a) the (column member) backbone moment-rotation curve and (b) the degradation parameters, which are depicted in Fig. 2b. The backbone can be defined by ($M_y$) the effective yielding moment, ($K_0$) the effective elastic stiffness, ($\alpha_s$) hardening to effective elastic stiffness ratio or strain hardening ratio, ($\Delta\theta_p$) pre-capping rotation, ($\Delta\theta_{pc}$) post-capping rotation. The degraded capacities are defined by ($\kappa$) the residual to yielding moment ratio $M_r/M_y$ and ($\theta_u$) the ultimate rotation capacity. The hysteretic degradation response is implemented by assigning $\lambda$ and $c$ for each deterioration mode (e.g., strength deterioration or unloading stiffness deterioration modes). The parameter D defines the rate of cyclic deterioration in the positive/negative loading direction and controls the (a)symmetry of the hysteretic behavior (a value equal to one

**Table 2**
Considered damage states (DSs), engineering demand parameters ($EDP_{DS}$), EDP capacity criteria ($EDP_{DS,c}$), and related formulations.

| damage level | low to moderate | | significant to sidesway collapse | | | | | |
|---|---|---|---|---|---|---|---|---|
| DS | $DS_{IDR,NSD}$ | $DS_{\theta y}$ | $DS_{IDR,SD}$ | $DS_{IDR,4\%}$ | $DS_{\theta u}$ | $DS_{Vbc,d}$ | $DS_{Vbc,b}$ | $DS_{RDRu}$ |
| $EDP_{DS}$ | IDR | θ | IDR | IDR | θ | $V_{bc}$ | $V_{bc}$ | RDR |
| $EDP_{DS,c}$ | $IDR_{NSD}$ | $\theta_y$ | $IDR_{SD}$ | $IDR_{4\%}$ | $\theta_{u,80\%}$ | $V_{u,bc,d}$ | $V_{u,bc,b}$ | $RDR_u$ |
| Equation | (2) | (3) | (4) | (5) | (6) | (9) | (10) | (11) |

**Table 3**
Seismic demand spectral acceleration corresponding to the building fundamental period Sa($T_1$) related to L'Aquila (AQ), associated with the respective limit states (LSs) and damage states (DSs).

| LS | DS | P [%] | $T_R$ [years] | Sa($T_1$) [g] | |
|---|---|---|---|---|---|
| | | | | A soil type | C soil type |
| **DLS** | $DS_{IDR,NSD}$<br>$DS_{\theta y}$ | 63% | 50 | 0.034 | 0.082 |
| **LSLS** | $DS_{IDR,SD}$<br>$DS_{IDR,4\%}$<br>$DS_{\theta u}$<br>$DS_{Vbc,d}$<br>$DS_{Vbc,b}$ | 10% | 475 | 0.107 | 0.212 |
| **$NCLS_1$** | $DS_{RDRu}$ | 5% | 975 | 0.146 | 0.261 |
| **$NCLS_2$** | | 2% | 2475 | 0.213 | 0.317 |
| **$NCLS_3$** | | NA[a] | NA[a] | 0.161 | 0.318 |

[a] $NCLS_3$ is not associated with values of P and $T_R$ since the related demand Sa($T_1$) was defined as 1.5 times LSLS demand, according to the approach provided in US building codes [22,52].

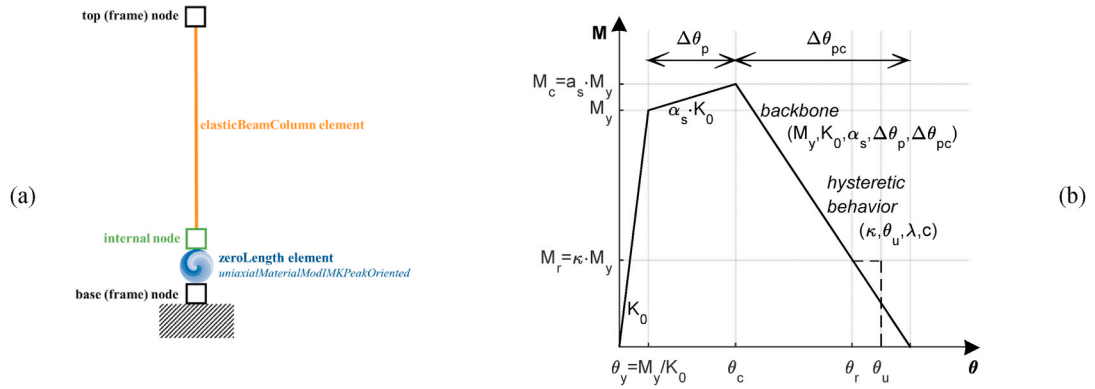


**Fig. 2.** (a) Schematic of the column series system and (b) backbone curve and degradation parameters related to peak-oriented hysteretic response model implemented through *uniaxialMaterial ModIMKPeakOriented*.

models a symmetric hysteretic response). The elastic behavior was assigned to the elastic element and elastic-plastic spring in such a way that (a) the (elastic) stiffness of the spring was equal to ten times the (elastic) stiffness of the elastic element and (b) the series response equaled the (member) backbone. This approach was derived from Ibarra and Krawinkler [56] and used in several recent studies (e.g. Refs. [25,31,36]).

The *uniaxialMaterial ModIMKPeakOriented* parameters have to be defined for a fixed value of the axial force since the model does not take into account the influence of its variation. The axial force corresponding to the seismic gravity loads was assigned. As it can be seen in Fig. 2b, the whole backbone pre-yielding behavior corresponds to a linear response and does not allow to define different pre- and post-cracking stiffnesses. Therefore, an effective elastic stiffness has to be defined for the pre-yielding branch.

The modeling parameters were derived from literature studies, favoring the use of formulations and calibrations relevant to precast columns (e.g. Ref. [39]). The yielding moment and curvature were estimated by performing a fiber analysis and assuming a bilinear idealized model. In particular, the constitutive behavior of the unconfined/confined concrete was modeled according to Mander et al. [59], while the stress-strain response of the steel rebars was derived from Eurocode 2 [28]. The failure of the cross-section was defined by the tension failure of the reinforcement, corresponding to a strain equal to 0.075 [28,39]. The pre-yielding branch of the bilinear idealized curve was defined by the first yielding of the rebars, whereas the slope of the post-yielding branch was defined according to the equal energy rule. The yielding rotation $\theta_y$ was evaluated according the formulation developed by Fardis and Biskinis [38]; the capping and post-capping rotations $\theta_c$ and $\theta_{pc}$ were derived from Haselton and Deierlein [41]. The formulations related to $\theta_y$, $\theta_c$, and $\theta_{pc}$ are consistent with the definition of $\theta_{u,80\%}$; in other words, the capacity associated with $\theta_{u,80\%}$ is assessed considering the backbone curve defined by $\theta_y$, $\theta_c$, and $\theta_{pc}$. The capping moment ($M_c$) was estimated according to the formulation provided by Haselton and Deierlein [41], which is reported in Equation (12).

$$\frac{M_c}{M_y} = 1.25 \cdot (0.89)^{\nu} \cdot (0.91)^{0.01 f_c'} \tag{12}$$

The residual moment ($M_r$) was set equal to zero, and the ultimate rotation ($\theta_u$) equaled the rotation associated with null moment on the backbone. The degradation parameter $\lambda$ was derived according to Equations (13) and (14). The formulation reported in Equation (13) was developed by Haselton and Deierlein [41]; in particular, s is the stirrup spacing, $V_p/V_n$ is the ratio between the shear demand

at yielding and the shear strength of the column, and $\rho_{sh,eff}$ is the effective ratio of the transverse reinforcement. $V_p$ was defined by the shear associated with the attainment of the capping moment at the base of the column, whereas $V_n$ was estimated according to NTC 2008 [26], i.e., according to the Ritter–Mörsch truss model. Equation (13) is consistent with the yielding rotation capacity considered by Haselton and Deierlein [41]. Therefore, the correction reported in Equation (14) was assumed in the present study to take into account the use of the formulation by Fardis and Biskinis [38] instead of the one considered by Haselton and Deierlein [41]. This correction was derived from Magliulo et al. [33]. The parameters c and D were assumed to be equal to one (for all degradation modes) and one, respectively (e.g. Ref. [33]).

$$\lambda' = 127.2 \cdot (0.19)^{\nu} \cdot (0.24)^{s/d} \cdot (0.595)^{V_p/V_n} \cdot (4.25)^{\rho_{sh,eff}} \tag{13}$$

$$\lambda = \lambda' \cdot (\theta_c - \theta_y) \tag{14}$$

### 3.3. Numerical analysis

Nonlinear static and dynamic analyses were performed considering the three-dimensional models and including the geometric nonlinearities (*P*-Δ effects [60]). The PO curves ($V_h$ versus RDR) were evaluated for both horizontal directions, and the $RDR_u$ capacities were estimated as it was defined in Section 3.1. Nonlinear dynamic analyses were carried out considering simultaneous actions along the horizontal directions and considering a MSA procedure [61,62]. The loading histories were derived from Refs. [25,63] according to the conditional spectrum (CS) approach [64,65]. The spectral acceleration (Sa) associated with the fundamental building period ($T_1$) was considered as an IM ($Sa(T_1)$). In particular, $T_1$ associated with the designed buildings was assumed to be equal to 2.0 s; this simplification was motivated by the fact that the case study buildings had fundamental periods relatively close to the abovementioned value (please, see Appendix A and also refer to RINTC project). MSA analyses were performed considering ten IM levels (or stripes), which corresponded to a return period ($T_R$) equal to 10, 50, 100, 250, 500, 1000, 2500, 5000, 10,000, and 100,000 years. 20 pairs of records were considered for each analysis stripe; the analysis records were selected among the Italian accelerometric archive ITACA (http://itaca.mi.ingv.it) and the NGAwest2 database (http://peer.berkeley.edu/ngawest2/). Fig. 3 depicts the spectral accelerations $Sa(T_1)$ related to the analysis IM levels and return periods $T_R$ for all considered sites and soil conditions.

### 3.4. Capacity assessment: fragility curves

The fragility associated with DS (i.e., $F_{DS}$) is defined as the probability that the structure/component exhibits DS for a given value of IM; in particular, the DS occurrence is associated with $EDP_{DS}$ exceeding or equaling the (EDP) capacity criterion $EDP_{DS,c}$. In the following, the fragility is expressed considering MSA approach and using $Sa(T_1)$ as an IM. $F_{DS}$ can be expressed as reported in Equation (15), where $\overline{Sa(T_1)}$ is a specific value of $Sa(T_1)$. $F_{DS}$ is typically modeled considering a lognormal distribution model (e.g. Ref. [66]), as it is reported in Equation (16), where Φ is the cumulative standard gaussian function, and $\mu_{DS}$ ($\sigma_{DS}$) is the mean (standard deviation) of the logarithm of $Sa(T_1)$ related to DS; $\mu_{DS}$ and $\sigma_{DS}$ are referred to in the following as logarithmic mean and standard deviation.

$$F_{DS} = P\left[EDP_{DS} \geq EDP_{DS,c} \,\middle|\, Sa(T_1) = \overline{Sa(T_1)}\right] \tag{15}$$

$$F_{DS} = \Phi\left[\frac{(\ln(\overline{Sa(T_1)}) - \mu_{DS}}{\sigma_{DS}}\right] \tag{16}$$

The fragility curves were estimated in the paper using the EDP-based approach since MSA analyses were performed (e.g. Refs. [67,68]). The fragility was computed considering multiple methods, i.e., (a) Shome and Cornell (i.e., 3Par (discrete) fragility) [69] (b) maximum likelihood fit (i.e., MLF fragility), [70] (c) normal probability paper fit (i.e., NPP fragility), [71], and (d) least squares fit (i.e.,

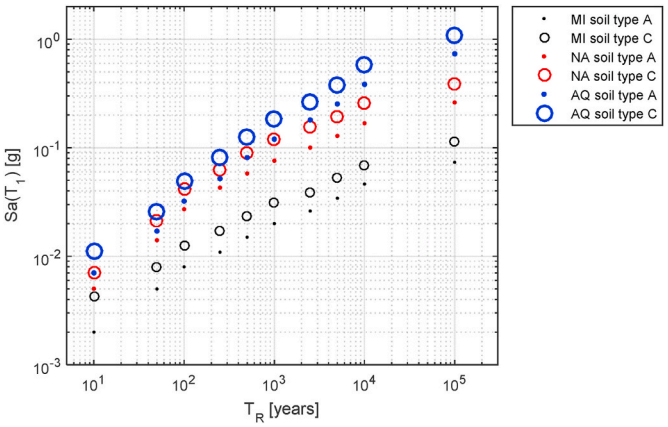


**Fig. 3.** Spectral acceleration corresponding to the fundamental vibration period ($Sa(T_1)$) associated with the multiple-stripe analysis (MSA) intensity measure (IM) levels and return periods ($T_R$) for all sites and soil conditions.

LSF fragility) [72].

The formulation provided by Shome and Cornell [69] follows a three-parameter model, based on the probability of non-collapse, and the mean/median and dispersion values conditioned on non-collapse (3Par fragility, Table 4). This fragility can be evaluated for the discrete IM values related to the MSA (i.e., analysis stripe IMs). In particular, the 3Par fragility $F_{DS,j}$, associated with DS and related to the jth analysis stripe, is reported in Equation (17). $|Sa(T_1)|_j$ is the $Sa(T_1)$ value corresponding to the jth analysis stripe, and $P_C$ ($P_{NC}$) is the probability of collapse (non-collapse) defined in Equation (18) ((19)), where collapse is meant as dynamic instability or non-convergence, $c_j$ is the number of collapse occurrences corresponding to the jth analysis stripe, $n$ is the number of analysis records; $\mu_{EDP_{DS}}$ and $\sigma_{EDP_{DS}}$ are the mean and standard deviation of $\ln(EDP_{DS,j})$, where $EDP_{DS,j}$ represents the $EDP_{DS}$ analysis results associated with the jth analysis stripe and related to non-collapse conditions.

$$F_{DS,j} = P\left[EDP_{DS} \geq EDP_{DS,c} \;\middle|\; Sa(T_1) = |Sa(T_1)|_j\right] = P_C + P_{NC}\left\{1 - \Phi\left[\frac{ln\left(EDP_{DS,c}\right) - \mu_{EDP_{DS,j}}}{\sigma_{EDP_{DS,j}}}\right]\right\} \tag{17}$$

$$P_C = \frac{c_j}{n} \tag{18}$$

$$P_{NC} = 1 - P_C \tag{19}$$

$\mu_{EDP_{DS,j}}$ and $\sigma_{EDP_{DS,j}}$ used to compute 3Par (discrete) fragility were evaluated according to Equations (20) and (21), respectively, where $EDP_{DS,j,i}$ is the ith $EDP_{DS}$ analysis result related to the jth analysis stripe (excluding the collapse conditions) associated with DS (e.g. Ref. [67]).

$$\mu_{EDP_{DS,j}} = \left(n - c_j\right)^{-1} \sum_{i=1}^{n-c_j} \ln\left(EDP_{DS,j,i}\right) \tag{20}$$

$$\sigma_{EDP_{DS,j}} = \sqrt{\left(n - c_j - 1\right)^{-1} \sum_{i=1}^{n-c_j} \left[\ln\left(EDP_{DS,j,i}\right) - \mu_{EDP_{DS,j}}\right]^2} \tag{21}$$

The maximum likelihood fit method [70] was based on the estimation of the fragility parameters $\mu_{DS}$ and $\sigma_{DS}$ according to Equation (22), considering Equation (16) for the definition of $F_{DS}$ (MLF fragility, Table 4). In Equation (22), $u$ is the number of analysis stripes, $q_j$ is the number of failures associated with the jth stripe (i.e., corresponding to $|Sa(T_1)|_j$). It should be noted that MLF formulation does not distinguish the influence of failure due to EDP threshold achievement and instability/non-convergence conditions. In these latter cases, collapses are also meant as EDP threshold achievements.

$$\{\mu_{DS}, \sigma_{DS}\} = \underset{\mu'_{DS},\, \sigma'_{DS}}{argmax}\left[\sum_{j=1}^{u}\left\{ln\binom{n}{q_j} + q_j\, ln\left\{\Phi\left[\frac{\ln\left(|Sa(T_1)|_j\right) - \mu'_{DS}}{\sigma'_{DS}}\right]\right\} + \left(n - q_j\right) ln\left\{1 - \Phi\left[\frac{\ln\left(|Sa(T_1)|_j\right) - \mu'_{DS}}{\sigma'_{DS}}\right]\right\}\right\}\right] \tag{22}$$

The normal probability paper fit [71] formulation was implemented by fitting the (discrete) 3Par fragility via least squares fitting on normal probability paper (Z versus $\ln(Sa(T_1))$) considering a line model (NPP fragility, Table 4). In particular, Z is a standard normal variable, which corresponds to the failure probabilities evaluated as reported in Equation (23), where $z_j$ is the failure probability associated with the jth stripe and $P[EDP_{DS} \geq EDP_{DS,c} | \; Sa(T_1) = \overline{Sa(T_1)}]$ is evaluated according to the 3Par method.

$$z_j = \Phi^{-1}\left(P\left[EDP_{DS} \geq EDP_{DS,c} \;\middle|\; Sa(T_1) = |Sa(T_1)|_j\right]\right) \tag{23}$$

The line fitting model over the normal probability paper is expressed in Equation (24), where the parameters $\sigma_{DS}$ and $\mu_{DS}$ can be estimated according to Equations (25) and (26), respectively. In particular, $\bar{z}$ and $\overline{\ln\left(Sa(T_1)\right)}$ can be evaluated according to Equations (27) and (28), respectively.

$$Z = -\frac{\mu_{DS}}{\sigma_{DS}} + \sigma_{DS}{}^{-1} \ln\left(Sa(T_1)\right) \tag{24}$$

**Table 4**
Considered fragility methods and related references.

| fragility method | Shome and Cornell (or three-parameter) | maximum likelihood fit | normal probability paper | least squares fit |
|---|---|---|---|---|
| method ID | 3Par | MLF | NPP | LSF |
| main reference | [69] | [70] | [71] | [72] |
| Equations | (17) to (20) | (16) and (22) | (17) to (21) and (23) to (28) | (16), (18) to (21), and (29) |

$$\sigma_{DS} = \frac{\sum_{j=1}^{u} \left(z_j - \overline{z}\right)^2}{\sum_{j=1}^{p} \left(z_j - \overline{z}\right) \left[\ln\left(|\mathrm{Sa}(T_1)|_j\right) - \overline{\ln\left(\mathrm{Sa}(T_1)\right)}\right]} \tag{25}$$

$$\mu_{DS} = \overline{\ln\left(\mathrm{Sa}(T_1)\right)} - \frac{\overline{z}}{\sigma_{DS}} \tag{26}$$

$$\overline{z} = u^{-1} \sum_{j=1}^{u} z_j \tag{27}$$

$$\overline{\ln\left(\mathrm{Sa}(T_1)\right)} = u^{-1} \sum_{j=1}^{u} \ln\left(|\mathrm{Sa}(T_1)|_j\right) \tag{28}$$

The least squares fitting method [72] is based on fitting the fragility function (LSF fragility, Table 4) by minimizing the sum of squared errors, as it is reported in Equation (29), where $P_{NC}$ ($P_C$), $\mu_{EDP_{DS,j}}$, and $\sigma_{EDP_{DS,j}}$ are estimated as reported before, i.e., according to the 3Par method. A summary of the considered methods and related information are reported in Table 4. The fragility methods were applied in the study using the R2R software [67].

$$\{\mu_{DS}, \sigma_{DS}\} = \underset{\mu', \sigma'}{argmin} \left[ \sum_{j=1}^{u} \left\{ P_{NC} \left\{ 1 - \Phi\left[ \frac{ln\left(EDP_{DS,c}\right) - \mu_{EDP_{DS,j}}}{\sigma_{EDP_{DS,j}}} \right] \right\} + P_C - \Phi\left[ \frac{\ln\left(|\mathrm{Sa}(T_1)|_j\right) - \mu'_{DS}}{\sigma'_{DS}} \right] \right\}^2 \right] \tag{29}$$

### 3.5. Performance evaluation: capacity margin ratios, failure probabilities, and reliability indexes

The collapse margin ratio ($Z_c$) is a primary parameter for the safety assessment of structures regarding collapse (e.g. Refs. [22,36,73]). $Z_c$ can be defined as the ratio between the collapse fragility median $m_c$, expressed as an IM value (i.e., $Sa(T_1)$), and the MCE IM value ($Sa(T_1)_{MCE,c}$) [22,52], as it reported in Equation (30). The US codes [22,52] provide the (risk-targeted) MCE ground motion spectral accelerations for the collapse margin assessment ($Sa(T_1)_{MCE}$) over the US territory. $Z_c$ can also be more generally defined as the ratio between the collapse IM level and a major design earthquake IM level (e.g., Level 2 [74] or Level 3 [75] earthquake according to the Japanese design code).

$$Z_c = \frac{m_c}{\mathrm{Sa}(T_1)_{\mathrm{MCE,c}}} \tag{30}$$

The assessment based on the (collapse) margin ratio could be extended to DSs and LSs not associated with collapse, and it would be expressed as it is shown in Equation (31), where $Z_{LS,DS}$ is the margin ratio related to LS, considering DS as a damage state, and $Sa(T_1)_{MCE,LS}$ is the associated LS MCE spectral acceleration.

Insights and technical comments on the risk-targeted MCE ground motions and related collapse assessment can be found in the studies by Haselton et al. [76] and Fajfar [77]. In the present study, $Sa(T_1)_{MCE,LS}$ was derived from the Italian demand acceleration spectra associated with the relevant PLs and LS, including the collapse condition, considering the specific site and soil conditions. In particular, $Sa(T_1)_{MCE,LS}$ was assumed to be equal to the reference seismic demand actions expressed as it was described in Section 3.1 [29,35] and reported in Table 3 for AQ site.

$$Z_{LS,DS} = \frac{m_{DS}}{\mathrm{Sa}(T_1)_{\mathrm{MCE,LS}}} \tag{31}$$

FEMA P695 [22] (section 7.2) recommends adjusting the numerically estimated collapse margin ratios in order to account for the discrepancy between the features of rare ground motions in Western US and the design spectrum provided by the US codes (ASCE/SEI 7–05) (please, refer to the study by Baker and Cornell [78]). In the specific context, the mentioned adjustment methodology is not applicable, and the authors believe that the collapse margin ratios estimated through the MSA are consistent with the associated seismic demand spectra; for more details, please, see Refs. [16,25,63].

The conditional failure probability associated with LS, considering DS as a criterion, ($P_{f,LS,DS}$) is a significant parameter to evaluate the safety of structures, and this is often assessed regarding the collapse as a DS. $P_{f,LS,DS}$ is expressed in Equation (32), where $\mathrm{Sa(T_1)_{MCE,LS}}$ expresses the LS seismic demand.

$$\mathrm{P_{f,LS,DS}} = \mathrm{P}\left[ EDP_{DS} \geq EDP_{DS,c} \,\middle|\, \mathrm{Sa}(T_1) = \mathrm{Sa}(T_1)_{\mathrm{MCE,LS}} \right] \tag{32}$$

It is worth noting that $P_{f,LS,DS}$ does not express the probability of DS failure over a period of time, which is a different parameter (i.e., $P_{f,DS,T}$), but it represents the probability that the building exhibits DS under the design spectral demand. The reliability indexes estimated in the literature and the target values reported by past studies/codes refer to $P_{f,DS,T}$; therefore, they cannot be considered as a reference in the present study since the reliability assessment is based on $P_{f,LS,DS}$.

The value of the acceptable (or target) LS-DS margin ratio ($Z^*_{LS,DS}$) is typically a function of (a) the uncertainty associated with the DS fragility assessment and (b) the target failure probability related to LS [22,79]. In particular, $Z^*_{LS,DS}$ can be evaluated as defined in

Equation (33), where $P^*_{f,LS}$ is the target failure probability associated with LS, which is considered to only depend on LS in this context. $P^*_{f,LS}$ is often defined for CLS by regulations and codes (e.g. Refs. [29,52]), and a value equal to 10% is typically considered for collapse assessment and NCLS [22,73]. In the present study, this value was extended to LSs other than NCLS due to the lack of literature and code references. This assumption errs on the side of caution since the lower damage LSs are associated with a $P^*_{f,LS}$ value related to the most severe damage LS. However, it would also be reasonable assuming that $P^*_{f,LS}$ could increase as the severity of LS decreases, as the strictness of the safety assessment would decrease. Values larger than 10% might be assumed for LSs other than NCLS. However, further studies should be carried out prior to make quantitative assumptions, and the authors believe that assuming $P^*_{f,LS}$ equal to 10% for all LSs is a reasonable choice, as it is consistent with code- and literature-based collapse assessment and is precautionary. The (tabular) collapse $Z^*_{LS,DS}$ values provided by FEMA P695 [22] correspond to the ones evaluated according to Equation (33).

$$Z^*_{LS,DS} = \exp\left(-\sigma_{DS} \cdot \Phi^{-1}\left(P^*_{f,LS}\right)\right) \tag{33}$$

A representative value of $\sigma_{DS}$ that also takes into account uncertainties that are additional to the record-to-record one (i.e., total uncertainty $\sigma_{tot}$) can be defined according to Ref. [22], i.e., as shown in Equation (34), where $\sigma$, $\sigma_{DR}$, $\sigma_{TD}$, and $\sigma_{MDL}$ represent the uncertainty associated with record-to-record variability, design requirements, test data, and modeling, respectively. $\sigma_{DR}$, $\sigma_{TD}$, and $\sigma_{MDL}$ were assumed to be equal to 0.30, which represents a representative value to be reasonably assumed for fair (or moderate) quality of the design requirements, test data, and modeling (e.g. Refs. [22,34]). In particular, the assumed value for $\sigma_{MDL}$ was consistent with the findings of Kramar et al. [80], who performed an accurate assessment of the modeling uncertainty associated with precast buildings.

$$\sigma_{TOT} = \sqrt{\sigma^2 + \sigma^2_{DR} + \sigma^2_{TD} + \sigma^2_{MDL}} \tag{34}$$

The reliability index associated with LS-DS ($\beta_{LS\text{-}DS}$) can be expressed as a function of $P_{f,LS,DS}$, as shown in Equation (35), and the acceptable reliability index only depends on LS in this study ($\beta^*_{LS}$). $\beta^*_{LS}$ can be found by assuming $P_{f,LS,DS}$ equal to $P^*_{f,LS}$ in Equation (35).

$$\beta_{LS,DS} = \Phi^{-1} \cdot \left(1 - P_{f,LS,DS}\right) \tag{35}$$

The lack of reference code and literature $\beta^*_{LS}$ values corroborates the use of Equation (35) for the estimation of $\beta^*_{LS}$, according to the relevant $P^*_{f,LS}$ values. This approach is more general and can be more easily extended to other applications where a different target probability ($P^*_{f,LS}$) is to be considered, e.g., according to more or less severe prescriptions. Fig. 4 depicts the reported correlations defined among the key performance evaluation parameters, expressed considering a generic DS and using $Sa(T_1)$ as an IM.

## 4. Results and discussion

### 4.1. Capacity assessment

Failure occurrences due to achievement of (a) EDP capacity thresholds ($N_{EDP}$) and (b) instability ($N_{ins}$) are reported in Appendix B. The fragility curves were estimated for all sites, soils, and geometry conditions, even though, in several cases, a significantly reduced or null number of failures were observed, especially considering significant to collapse DSs and MI and NA sites. $F_{DS}$ is depicted as a function of $Sa(T_1)$ considering the investigated methods (3Par, MLF, NPP, and LSF), for SS and LS geometries and A and C soil types.

Fig. 5 shows the results related to $DS_{IDR,NSD}$, corresponding to (1) NA and (2) AQ sites. The other cases but MI site-SS geometry-C soil type did not show meaningful results (i.e., $F_{DS}$ was approximately null for all IM levels). Concerning $DS_{IDR,NSD}$ (IDR-based damage of nonstructural components, IDR = 1%), MI site-SS geometry-C soil case is associated with a median $m_{DS}$ (logarithmic standard deviation $\sigma_{DS}$) equal to 0.109 and 0.106 g (0.152 and 0.146) considering NPP and LSF methods, respectively, whereas the only meaningful 3Par (empirical) $F_{DS}$ value (i.e., larger than 0.003 g) is equal to 0.691 and is related to $Sa(T_1)$ equal to 0.114 g; it was not possible to estimate the fragility according to MLF method. Considering $DS_{IDR,NSD}$ and AQ site, MLF and LSF fragilities are almost coinciding and match very well 3Par fragilities, whereas NPP one is slightly higher (lower) than these latter for C (A) soil type

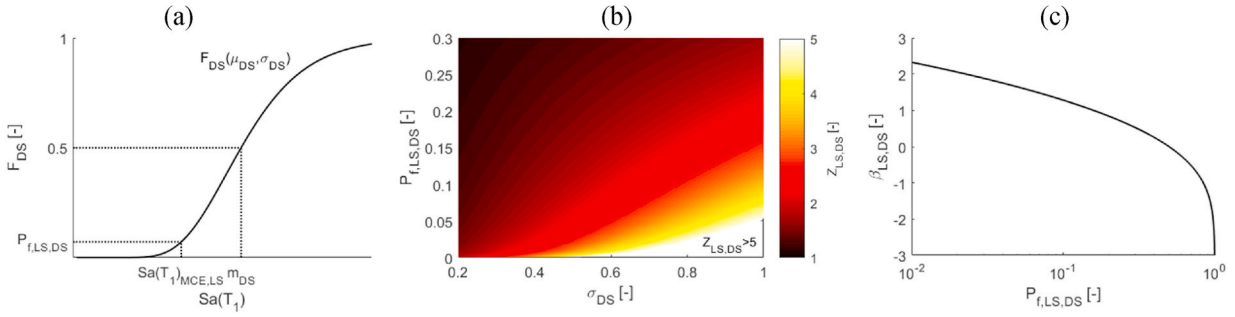


**Fig. 4.** Graphical correlations among the main performance evaluation parameters for a generic damage state (DS): (a) fragility curve ($F_{DS}$ versus $Sa(T_1)$) having median $m_{DS}$, logarithmic standard deviation $\sigma_{DS}$), maximum considered earthquake (MCE) $Sa(T_1)$ expressed as $Sa(T_1)_{MCE,LS}$, and failure probability $P_{f,LS,DS}$, (b) $P_{f,LS,DS}$ as a function of $\sigma_{DS}$ and capacity margin $Z_{LS,DS}$ (equal to $m_{DS}/Sa(T_1)_{MCE,LS}$), and (c) reliability index $\beta_{DS}$ as a function of $P_{f,LS,DS}$.

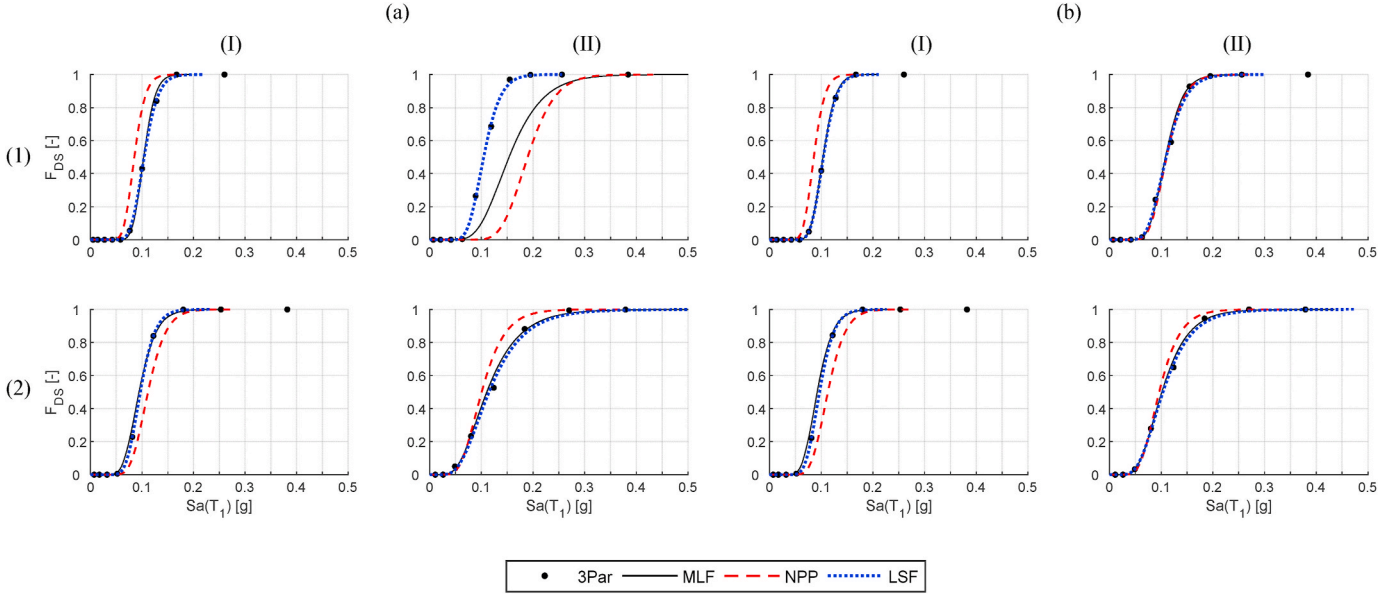


**Fig. 5.** Fragility curves ($F_{DS}$ versus $Sa(T_1)$) evaluated according to different methods (Shome and Cornell or three-parameter, i.e., 3Par; maximum likelihood fit, i.e., MLF; normal probability paper, i.e., NPP; least squares fit, i.e., LSF), related to $DS_{IDR,NSD}$, considering (1) Napoli (NA) site and (2) L'Aquila (AQ) site, (a) short-span (SS) and (b) long-span (LS) geometries, and (I) A and (II) C soil types. The fragility curves are reported up to $F_{DS}$ equal to 0.9999.

buildings. For the case of NA site, again MLF and LSF fragilities almost coincide, except for SS geometry and C soil type, where the LSF fragility is higher than MLF one. NPP fragility coincides with MLF and LSF fragilities for LS geometry and C soil type, whereas it is higher (lower) than MLF and LSF fragilities for both geometries and A soil type (SS geometry-C soil type). Both MLF and LSF fragilities match very well 3Par fragilities in all cases except SS geometry-C soil type, where only LSF fragility curve fits the 3Par fragilities. Considering the only MI site meaningful case, MLF and LSF methods supply approximately coinciding fragilities, which match very well the only 3Par fragility point. Except for the case of SS geometry-C soil type, and the not meaningful cases related to MI site, MLF and LSF medians related to all buildings essentially coincides, despite the different site and geometry, whereas the curve dispersions associated with C soil type cases is overall slightly larger than the one related to A soil type. Therefore, the design provisions related to the different site and the different building geometry do not overall affect the fragility of the buildings regarding the IDR-based damage of nonstructural elements (i.e., $DS_{IDR,NSD}$).

Regarding $DS_{\theta y}$ (yielding member end chord rotation), it was found that the IDR thresholds associated with this DS were quite similar to $IDR_{SD}$ (IDR-based severe structural damage, IDR = 2%). This makes $IDR_{SD}$ not consistent with severe damage but with first rotational yielding condition. Accordingly, $IDR_{SD}$ is found to be largely conservative (as it may be expected by code design using simplified methods). Such evidence is highlighted also in Deyanova et al. [81] and Ercolino et al. [1], where a typical Italian existing RC precast building is assessed. In the cited study, the slenderness of columns ensures a very high deformability in the elastic range, up to an IDR equal to about 2%. Therefore, the fragility curves related to $DS_{\theta y}$ are not depicted but only briefly described in the following. In particular, Table 5 shows the IDR thresholds related to $DS_{\theta y}$ computed for all considered case studies. It is worth specifying that the yielding condition in terms of member end chord rotation ($\theta \geq \theta_y$) was computed considering the global member end chord rotation and not the spring rotation. In fact, the yielding attainment assessed according to this latter series element is not representative of the actual yielding conditions of the structural member; as a matter of fact, the elastic stiffness of the spring and elastic element are conventional aliquots of the member's one, which corresponds to the global element's one. According to Table 5, the IDR associated to the first rotational yielding of all the code-compliant buildings is quite similar to the ones related to existing precast buildings having comparable layout. Moreover, yielding IDR does not significantly depend on site, geometry, and soil conditions. The findings also confirm that the yielding formulation adopted in this paper is consistent with the earlier code formulations. Further comments are omitted, and the reader is kindly referred to cited literature and Table 5.

Only AQ site fragilities associated with $DS_{\theta y}$ were relatively significant (e.g., 3Par $F_{DS}$ larger than 0.20), whereas a limit case was observed regarding NA site-C soil type buildings. In particular, only MLF and LSF fragilities related to LS geometry produced meaningful results, e.g., fitted $F_{DS}$ compatible with not null 3Par $F_{DS}$, overall comparable with AQ site. Regarding NA site-SS geometry-C soil type, 3Par $F_{DS}$ was smaller than NA site-C soil type case one, but still not null, and all fitting methods did not provide meaningful $F_{DS}$. The different methods produced a significant discrepancy among AQ site buildings. In particular, considering A (C) soil type, MLF and NPP (NPP and LSF) fragilities were quite similar and LSF (MLF) fragility was significantly lower (higher). Considering AQ site, (only) MLF fragility medians were not conditioned by the different geometry and soil type, whereas soil conditions affect $\sigma_{DS}$. LSF fragility curves were the ones that fitted more reasonably the 3Par fragilities. Both medians and logarithmic standard deviations, estimated according to the different methods, were more comparable among them for A soil type buildings, and both parameters were significantly lower than C soil type buildings ones.

Fragility curves for the case of $DS_{IDR,SD}$ (IDR-based significant damage) are reported in Fig. 6, for (1.1) NA and (1.2) AQ sites. MLF and LSF provide almost overlapped curves for both NA and AQ site buildings, except for AQ site-SS geometry-C soil type. However, in this case, LSF fragility is slightly lower than the MLF one. As concerns NPP methodology, the only case in which the provided fragility coincides with the others is AQ site-A soil type. For soil type C, they are always higher than the ones provided by the other two methods, for both the sites (with larger discrepancy for AQ site case) and both geometries. For the case of NA site-A soil type, NPP curves are below the other two for both geometries. However, differences are very small and reflect in the values of the median $m_{DS}$, which is quite similar over all methodologies. A higher NPP-MLF/LSF discrepancy in terms of $m_{DS}$ is detected for the cases of AQ site-LS geometry-C soil type, i.e., NPP to MLF $m_{DS}$ difference about 16%. 3Par fragilities do not match the curves provided by the other three methods over higher intensities, especially for C soil type cases. Outcomes from the case of MI site do not show any significance, since no failure occurs. Furthermore, MLF method is not able to find numerical solutions for all the MI site cases.

Fig. 6.2 illustrates the resulting fragilities for the case of $DS_{IDR,4\%,}$ (IDR = 4%) only for AQ site. Indeed, for NA and MI sites, the number of failure cases is not adequate to ensure a reliable evaluation and acceptable results. The curves are quite similar among the different methods. For the cases of A soil type, the highest curve is provided by MLF method, followed by the LSF and NPP; for the case of soil type C, the highest curve is always the NPP one, followed by the LSF and the MLF (MLF and LSF) for SS (LS) geometry. However, geometry does not affect median values, whereas C soil type is associated with medians higher than the ones provided by A soil type cases. The largest variation among all methodologies is equal to about the 13% (corresponding to SS geometry-C soil type). Fitted curve

**Table 5**
IDR thresholds associated with $DS_{\theta y}$ corresponding to the investigated case studies.

| site | | MI | | | | NA | | | | AQ | | | |
|---|---|---|---|---|---|---|---|---|---|---|---|---|---|
| geometry | | SS | | LS | | SS | | LS | | SS | | LS | |
| soil type | | A | C | A | C | A | C | A | C | A | C | A | C |
| IDR [−] | X dir | 0.0199 | 0.0200 | 0.0193 | 0.0188 | 0.0208 | 0.0200 | 0.0192 | 0.0183 | 0.0208 | 0.0177 | 0.0192 | 0.0186 |
| | Z dir | 0.0216 | 0.0213 | 0.0202 | 0.0203 | 0.0222 | 0.0213 | 0.0206 | 0.0193 | 0.0222 | 0.0189 | 0.0206 | 0.0200 |

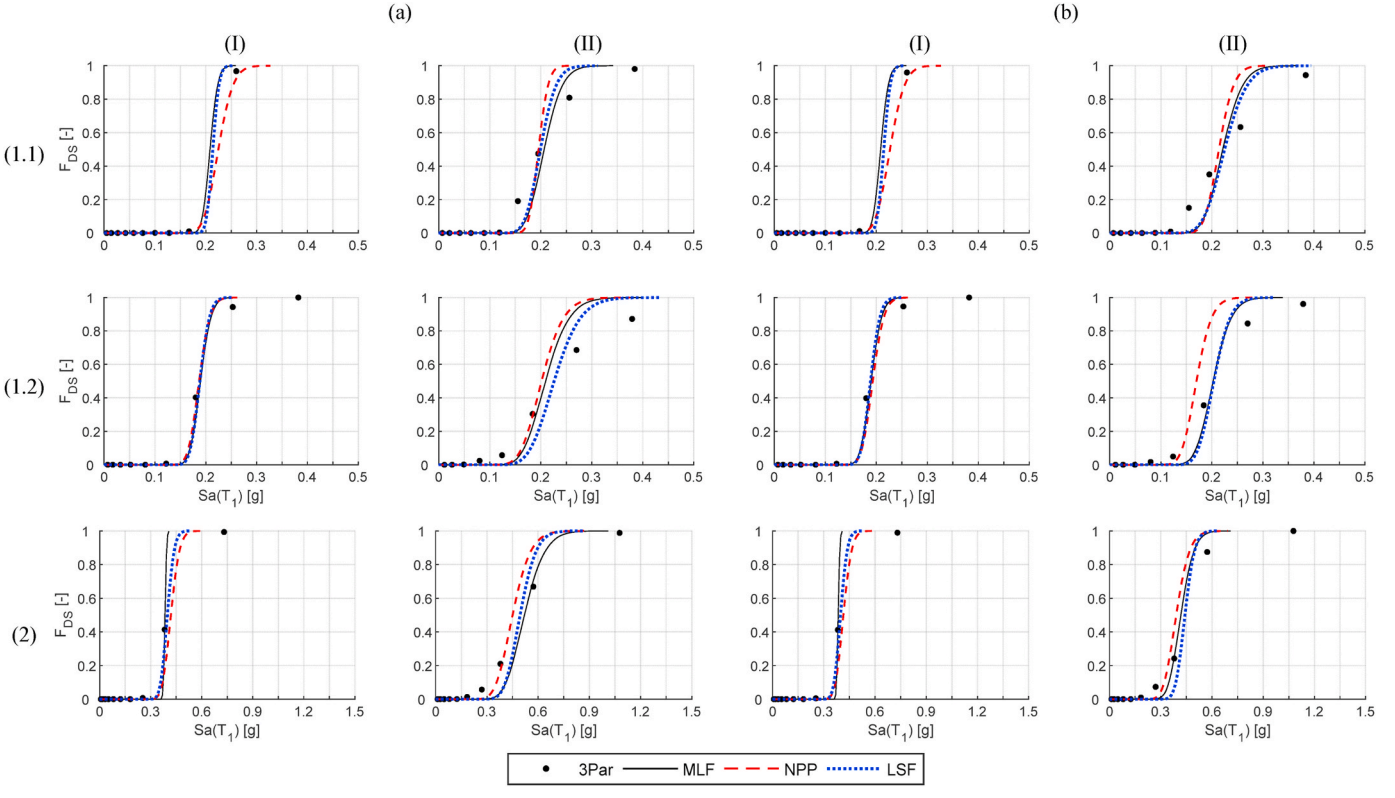


**Fig. 6.** Fragility curves ($F_{DS}$ versus $Sa(T_1)$) evaluated according to different methods (Shome and Cornell or three-parameter, i.e., 3Par; maximum likelihood fit, i.e., MLF; normal probability paper, i.e., NPP; least squares fit, i.e., LSF), related to (1.1) $DS_{IDR,SD}$ and Naples (NA) site, (1.2) $DS_{IDR,SD}$ and L'Aquila (AQ) site, and (2) $DS_{IDR,4\%}$ and L'Aquila (AQ) site, (a) short-span (SS) and (b) long-span (LS) geometries, and (I) A and (II) C soil types. The fragility curves are reported up to $F_{DS}$ equal to 0.9999.

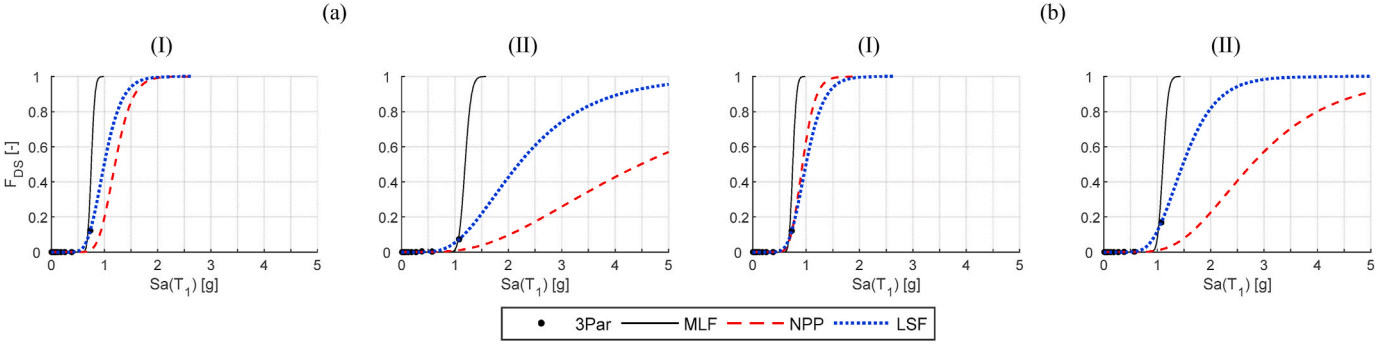


**Fig. 7.** Fragility curves ($F_{DS}$ versus $Sa(T_1)$) evaluated according to different methods (Shome and Cornell or three-parameter, i.e., 3Par; maximum likelihood fit, i.e., MLF; normal probability paper, i.e., NPP; least squares fit, i.e., LSF), related to $DS_{0u}$ and L'Aquila (AQ) site, (a) short-span (SS) and (b) long-span (LS) geometries, and (I) A and (II) C soil types. The fragility curves are reported up to $F_{DS}$ equal to 0.9999.

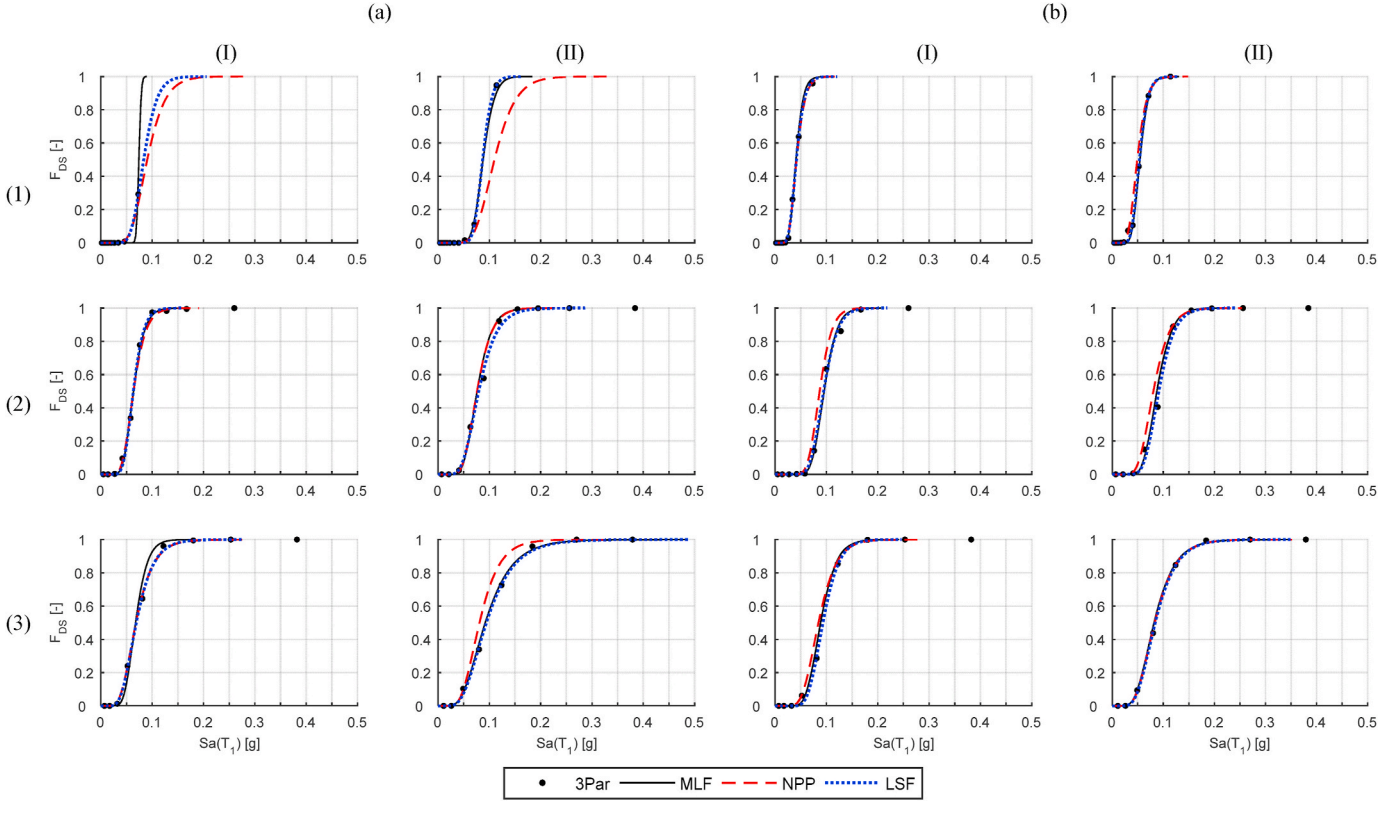


**Fig. 8.** Fragility curves ($F_{DS}$ versus $Sa(T_1)$) evaluated according to different methods (Shome and Cornell or three-parameter, i.e., 3Par; maximum likelihood fit, i.e., MLF; normal probability paper, i.e., NPP; least squares fit, i.e., LSF), related to $DS_{Vbc,b}$, considering (1) Milan (MI), (2) Naples (NA), and (3) L'Aquila (AQ) sites, (a) short-span (SS) and (b) long-span (LS) geometries, and (I) A and (II) C soil types. The fragility curves are reported up to $F_{DS}$ equal to 0.9999.

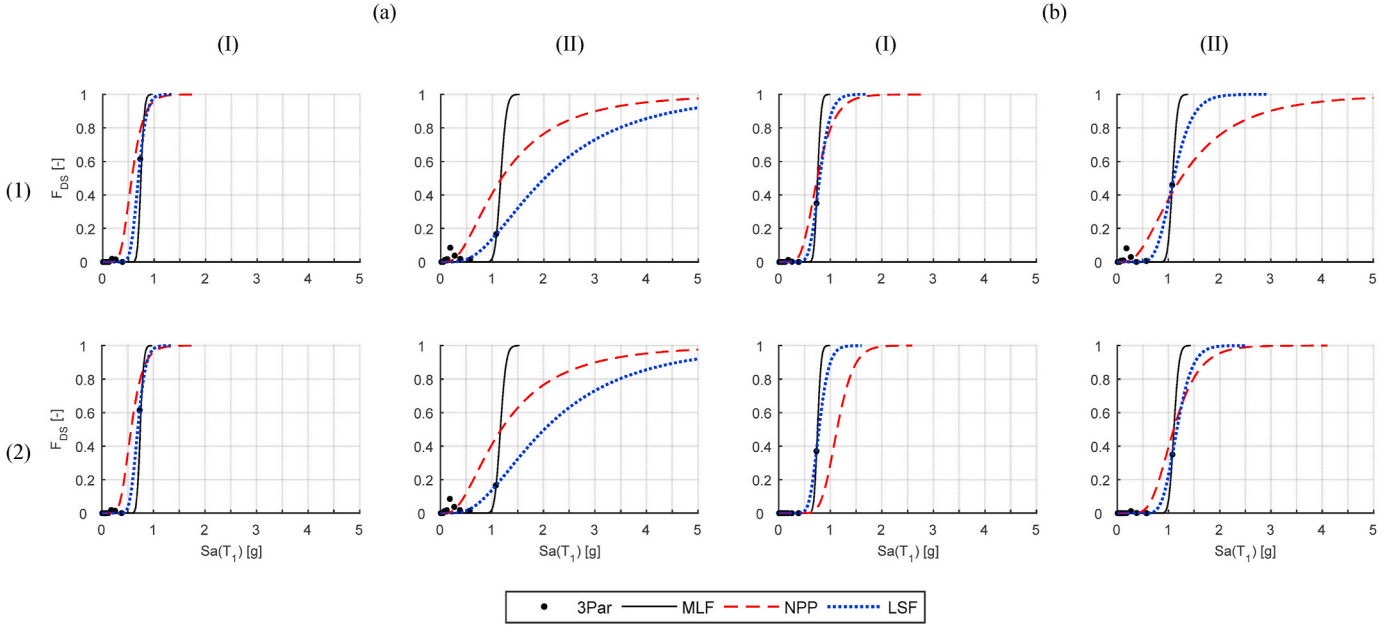


**Fig. 9.** Fragility curves ($F_{DS}$ versus $Sa(T_1)$) evaluated according to different methods (Shome and Cornell or three-parameter, i.e., 3Par; maximum likelihood fit, i.e., MLF; normal probability paper, i.e., NPP; least squares fit, i.e., LSF), related to (1) $DS_{Vbc,d}$ and (2) $DS_{RDRu}$, considering L'Aquila (AQ) site, (a) short-span (SS) and (b) long-span (LS) geometries, and (I) A and (II) C soil types. The fragility curves are reported up to $F_{DS}$ equal to 0.9999.

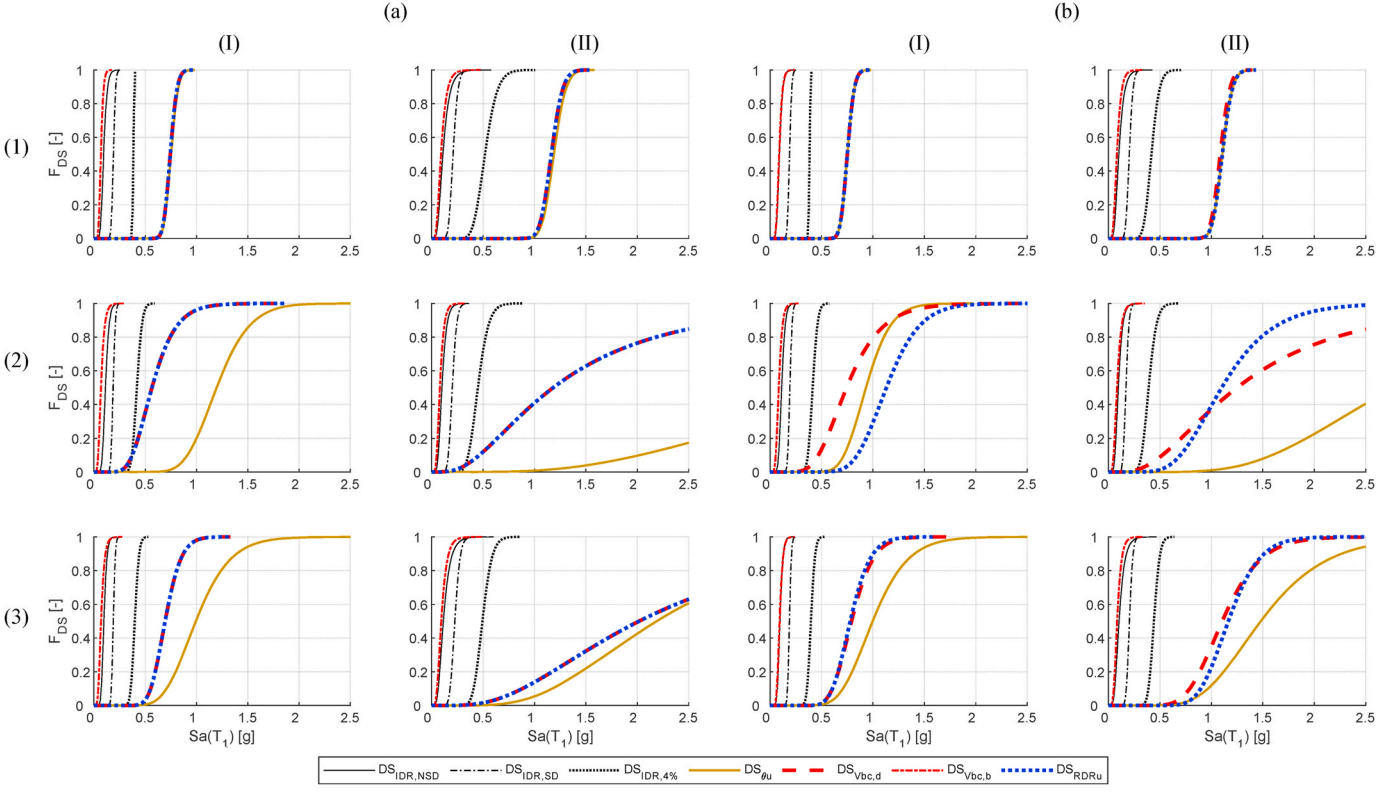


**Fig. 10.** Fragility curves ($F_{DS}$ versus $Sa(T_1)$) related all damage states (DSs) evaluated for L'Aquila (AQ) site, according to (1) maximum likelihood fit, i.e., MLF, (2) normal probability paper, i.e., NPP, and (3) least squares fit, i.e., LSF methods, considering (a) SS and (b) LS geometries, and (I) A and (II) C soil types. The fragility curves are reported up to $F_{DS}$ equal to 0.9999.

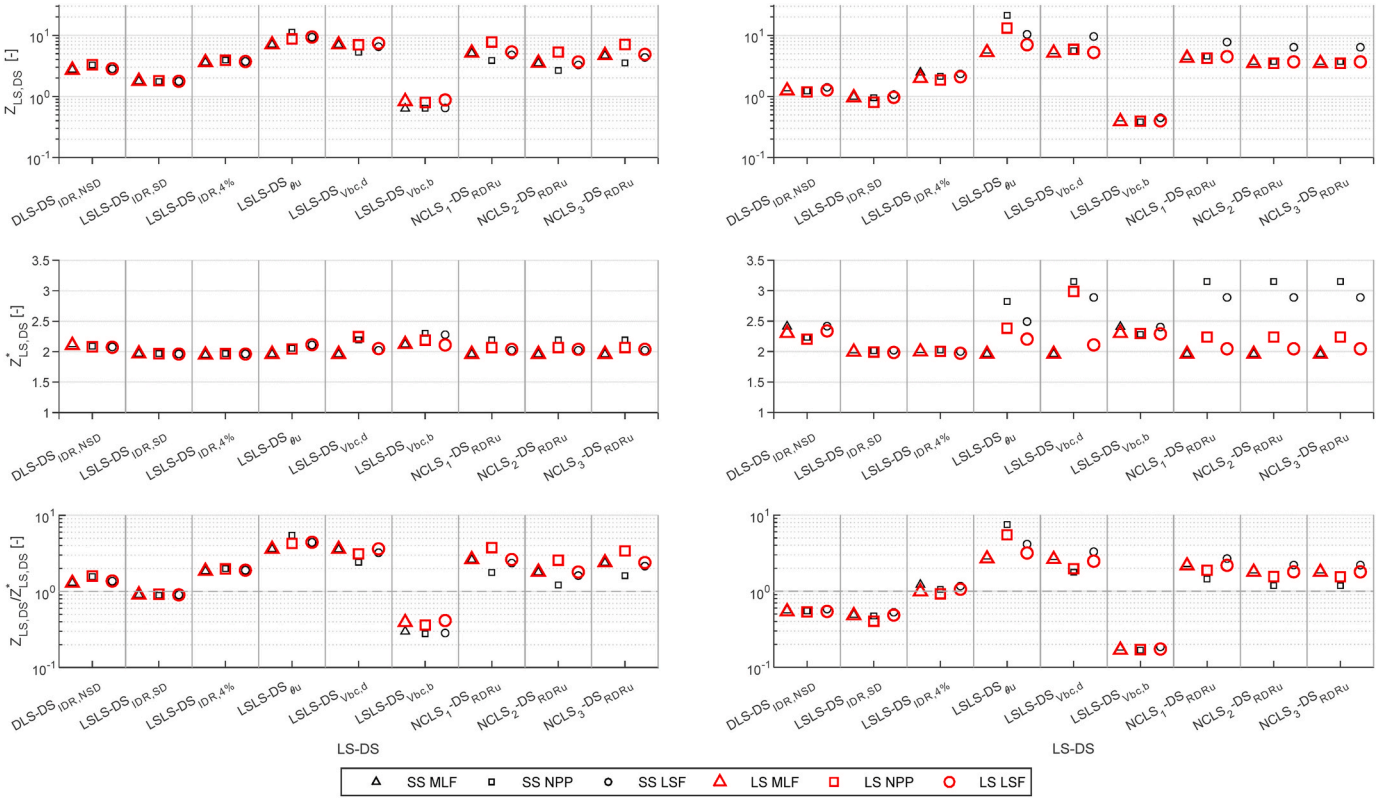


**Fig. 11.** Capacity margin ($\mathbf{Z}_{LS,DS}$), target capacity margin ($Z^*_{LS,DS}$), and capacity margin to target capacity margin ratio ($\mathbf{Z}_{LS,DS}/Z^*_{LS,DS}$) as a function of the different limit state-damage states (LS-DS) case, considering L'Aquila (AQ) site and short-span (SS) and long-span (LS) geometries, for soil type (a) A and (b) C, according to maximum likelihood fit (MLF), normal probability paper (NPP), and least squares fit (LSF) methods. The grey dashed line depicts the unitary value of the $\mathbf{Z}_{LS,DS}/Z^*_{LS,DS}$ ratio.

fragilities trace better 3Par data for A soil type, if compared with C soil type ones, in which the dispersion is always higher.

The outcomes related to $DS_{\theta u}$ (ultimate member end chord rotation) are reported in Fig. 7, only for the meaningful conditions, i.e., AQ site cases. Overall, MLF and LSF match very well 3Par fragilities, which are only defined for low $F_{DS}$ (i.e., lower than 0.20). The highest fragilities, i.e., the most conservative, are always the MLF ones, followed by the LSF and NPP, except for the case of LS geometry-A soil type, in which NPP is slightly higher than LSF. C soil type cases always provide curves with higher dispersion, especially for NPP method, which is very far from 3Par estimations. The dispersion of fragility curves related to A soil type are significantly lower than (equal to) C soil type ones for NPP and LSF (MLF) methods. It should be noted that $DS_{\theta u}$ fragility assessment is affected by the peculiar case of failure occurrences only corresponding to one (the highest) IM level. This results in potentially unreliable estimations, especially for NPP that provides extremely low fragilities.

The fragility curves related to $DS_{Vbc,b}$ (dowel connections brittle shear failure) are shown in Fig. 8. The applied fragility methods provide very similar curves for all cases, due to the high number of failure occurrences, with only few exceptions: MI site-SS geometry. In such cases, NPP fragility is lower than the other two. It is worth noting that the non-negligible dispersion among the different curves related to MI site-SS geometry-A soil type is associated to a low number of collapses (only 8/40 for IM10); however, the different fitted curves match very well 3Par fragilities. For MI site-SS geometry-C soil type, NPP fragility does not fit well the IM10 3Par fragility, differently from the other two methods. The extremely high fragility related to $DS_{Vbc,b}$ confirms that a brittle connection failure should be avoided by providing adequate structural details: the associated capacity of the building is even lower than the yielding capacity (the comparison could be made considering $DS_{IDR,SD}$ fragilities, which are quite similar to $DS_{\theta y}$). The soil condition is not found to affect significantly the fragility, whereas geometry conditions the fragility in some cases (without a clear trend). As the seismicity increases, overall the fragility related to $DS_{Vbc,b}$ slightly decreases, even though without a regular pattern.

Fig. 9.1 reports fragilities for $DS_{Vbc,d}$ (dowel connections ductile shear failure), only for AQ site. Curves show an irregular trend, intersecting each other in different points. 3Par fragilities do not increase monotonically as the IM level grows, especially for C soil type; however, the fragility of IM levels lower than 10 has extremely low values. NPP curves do not match very well 3Par fragilities for SS geometry (IM 10 level), whereas all methods are quite close to 3Par fragilities for LS geometry. The highest dispersion is detected for C soil type cases. Since failures only occur corresponding to IM10, as it was also observed for $DS_{\theta u}$, only the 3Par fragility associated with this stripe is significant, and this does not allow to assess the robustness of the fitting curves. Considering MLF method, geometry does not affect the results, whereas soil type C produces a fragility significantly lower than soil type A. Similar considerations can be drawn for the last case, reported in Fig. 9.2, that is $DS_{RDR,u}$ (RDR corresponding to the 50% degradation in the maximum global shear, i.e., sidesway-like collapse). Again, only outcomes for AQ site are reported. For the SS geometry, fragilities are exactly the same of the $DS_{Vbc,d}$, due to the identical number and type (EDP-based or numerical instability) of failures. The only anomaly is associated with LS geometry, especially for soil type A where NPP fragility related to $DS_{RDR,u}$ is lower than the $DS_{Vbc,d}$ one.

In Fig. 10, a comparison among all the considered damage states for AQ site is reported. Starting with the MLF method, the observed DS sequence is the same for all the geometries and the soil types, and it is consistent with the expectations. The highest curve, providing the lowest median value, is the one related to the brittle failure of the dowel connections, confirming the extreme danger related to this kind of collapse; then, it can be found in order: IDR-based non-structural damage, IDR-based significant damage (IDR = 2%), 4% IDR-based, and, in the end, all overlapped, the ductile failure of dowel connections, RDR corresponding to the sidesway-like condition and the plastic hinges ultimate chord rotation. For the other two methods, i.e., NPP and LSF, an anomaly is detected, since the $DS_{\theta u}$ fragility follows the $DS_{RDR,u}$ one, for all the cases, except LS geometry-A soil type for the NPP method. This is not compatible with the modeling assumptions since a correspondence between the top drift and the plastic hinges rotation should be verified; as a matter of fact, the building has single-story, the beam-to-column connections are modeled as hinges, and a rigid diaphragm constrain is applied to the deck.

However, it is worth remembering that these latter methods were already found to be not particularly reliable and consistent, corresponding to a reduced number of failures, especially when these failures were observed only for one IM level.

### 4.2. Performance evaluation

The seismic performance was evaluated only considering AQ site since there was a limited or null number of observed failures corresponding to other sites, and this would have affected the significance and the reliability of the estimations (please, also see Section 4.1) (e.g. Ref. [36]). It is recalled that the performance evaluation accounts for uncertainty sources additional to the record-to-record one, as it was described in Section 3.5.

$Z_{LS,DS}$, $Z^*_{LS,DS}$, and $Z_{LS,DS}$ to $Z^*_{LS,DS}$ ratios are depicted in Fig. 11. The results are shown considering (a) A and (b) C soil type. Comments on $Z_{LS,DS}$ are omitted for the sake of brevity since the $Z_{LS,DS}$ to $Z^*_{LS,DS}$ is more consistent as an evaluation parameter. Moreover, $Z^*_{LS,DS}$ values are not significantly dispersed, unless few peculiar cases are considered. Considering A soil type, $Z^*_{LS,DS}$ is not significantly conditioned by different fragility methods and investigated LS-DS conditions, and the values are overall approximately equal to about 2. A different trend is found regarding C soil type, characterized by a more significant discrepancy among the different LS-DS conditions, geometries, and fragility methods. In particular, $Z^*_{LS,DS}$ associated with combination of SS geometry and NPP/LSF methods was significantly higher than the ones related to the other cases for some of LSLS-DS (LSLS-$DS_{\theta u}$, LSLS-$DS_{Vbc,d}$) conditions and all NCLS (NCLS$_1$-$DS_{RDRu}$, NCLS$_2$-$DS_{RDRu}$, and NCLS$_3$-$DS_{RDRu}$) conditions. This discrepancy might reasonably be a symptom of the not highly consistent estimation of the fragility related to limited failure occurrences. For further comment, the reader is kindly referred to Section 4.1.

$Z_{LS,DS}$/ $Z^*_{LS,DS}$ is larger than the unity (about 1.5) considering DLS-$DS_{IDR,NDS}$ for A soil type, whereas this ratio is significantly lower than the unity (about 0.5) considering C soil type. Accordingly, the design requirements do not seem to have provided an adequate

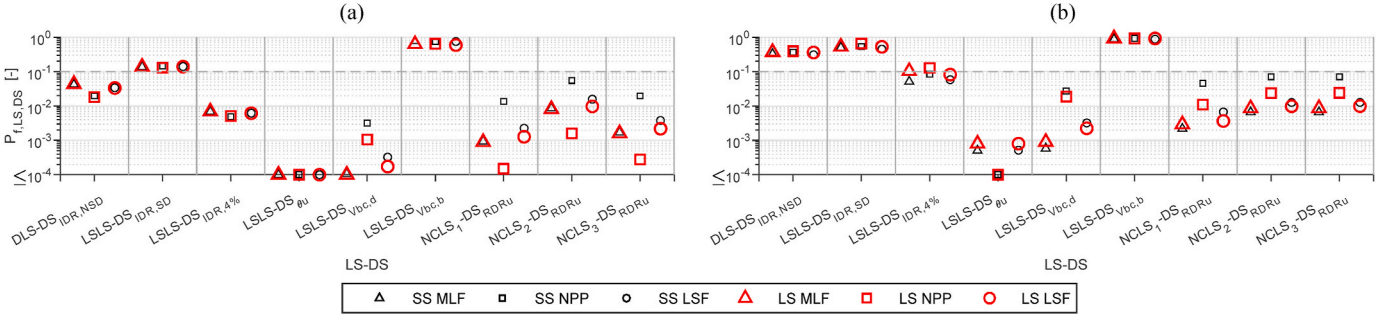


**Fig. 12.** Failure probability ($P_{f,LS,DS}$) as a function of the different limit state-damage state (LS-DS) case, considering L'Aquila (AQ) site and short-span (SS) and long-span (LS) geometries, for soil type (a) A and (b) C, according to maximum likelihood fit (MLF), normal probability paper (NPP), and least squares fit (LSF) methods. The grey dashed line depicts the target LS failure probability ($P^{*}_{LS}$).

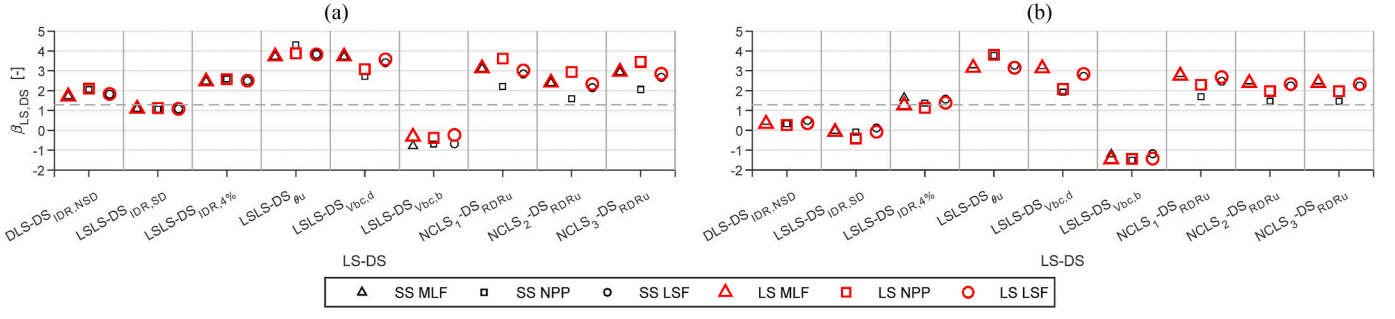


**Fig. 13.** Reliability index ($\beta_{LS,DS}$) as a function of the different limit state-damage states (LS-DS) case, considering L'Aquila (AQ) site and short-span (SS) and long-span (LS) geometries, for soil type (a) A and (b) C, according to maximum likelihood fit (MLF), normal probability paper (NPP), and least squares fit (LSF) methods. The grey dashed line depicts the target LS reliability index ($\beta^*_{LS}$).

building performance corresponding to DLS in the case of C soil type. Considering A soil type building as a reference, the design process did not determine an increment of buildings' capacities that is consistently balanced with the higher seismic demand for C soil type. The codes should provide stricter requirements regarding this soil condition. Regarding LSLS-$DS_{IDR,SD}$, the building performance is not adequate for both soil types, even though $Z_{LS,DS}/\ Z^*_{LS,DS}$ is just lower than the unity (about 0.9) for A soil type. It should be noted that $DS_{IDR,SD}$ is related to a relatively reduced level of damage (i.e., IDR equal to 2%) considering PLs associated with LSLS,

Especially comparing this DS with other LSLS-DS conditions (please, also see Fig. 10). Therefore, code prescriptions seem to be too conservative, and it would be probably more appropriate considering DLS demand when $DS_{IDR,SD}$ is assessed or a more consistent IDR threshold (i.e., larger than 2%) should be associated with severe damage DSs for LSLS PLs. Furthermore, a more adequate performance, which in some cases is extremely high, is found regarding more severe LSLS and NCLS conditions, except for LSLS-$DS_{Vbc,b}$ (Fig. 10). The extremely poor building performance regarding $DS_{Vbc,b}$ ($Z_{LS,DS}/\ Z^*_{LS,DS}$ equal to about 0.3–0.4 and 0.2 considering A and C soil type respectively) was expected since the associated building capacities were found to be very small and the seismic demand is related to LSLS. This enforces the need for preventing the conditions that favor the mechanism associated with this brittle connection failure (please, see Section 2). The building performance related to LSLS-$DS_{IDR,4\%}$ is amply satisfactory for A soil type, whereas the performance is just adequate or slightly inadequate considering C soil type. This stresses further the weakness already evidenced regarding DLS-$DS_{IDR,NDS}$ and LSLS-$DS_{IDR,SD}$. Considering LSLS-$DS_{Vbc,d}$ and all NCLS cases, the building overall showed an adequate performance. In particular, the performance related to LSLS-$DS_{Vbc,d}$ is found to be considerably higher than the one associated with NCLS cases. This evidence seems to be consistent with the fact the former and the latter DSs are associated with local (at the beam-to-column connection level) and global mechanisms, respectively. In fact, the connection is typically designed considering the capacity design approach. Furthermore, collapse failure should be associated with higher performance, also meant as failure probability. Nevertheless, the case study consists in code-conforming regular single-story buildings, and it is not expectable a major difference in terms of consequences between local and global failure mechanisms.

The different geometry of the buildings affects the capacity margin ratios in some cases, depending on both DS and fragility method. Overall, the most significant influence of the geometry is associated with NPP method. There is only one case in which the different geometry determines different outcomes in terms of performance adequacy. This case is related to LSLS-$DS_{IDR,4\%}$ and C soil type, where NPP method-SS geometry and NPP method-LS geometry present $Z_{LS,DS}/\ Z^*_{LS,DS}$ just higher and lower than the unity, respectively. In the other cases, even though the difference between the SS to LS geometry ratios was relatively significant, both estimations were associated with adequate or inadequate performances.

$P_{f,LS,DS}$ ($\beta_{LS,DS}$) and related target value $P^*_{LS}$ ($\beta^*_{LS}$) are depicted in Fig. 12 (Fig. 13), considering (a) A and (b) C soil type. As $P^*_{LS}$ ($\beta^*_{LS}$) is correlated to $Z^*_{LS,DS}$, the conditions related to $P_{f,LS,DS} > P^*_{LS}$ ($\beta_{LS,DS} < \beta^*_{LS}$) are equivalent to the condition $Z_{LS,DS}/\ Z^*_{LS,DS} < 1$, and associated comments related to Fig. 12 (Fig. 13) are referred to Fig. 11 for the sake of brevity. Neglecting the peculiar case of LSLS-$DS_{Vbc,b,}$ the design process determined critically unsafe performances regarding LSLS-$DS_{IDR,SD}$ for A soil type and both DLS-$DS_{IDR,NSD}$ and LSLS-$DS_{IDR,SD}$ for C soil type; for C soil type, MLF and NPP estimations associated with LS geometry produce a slightly unsafe performance for LSLS-$DS_{IDR,4\%}$. Moreover, extremely uneconomic performances are observed for some LSLS-DS and NCLS-DS conditions, especially for A soil type. This is evident by observing $P_{f,LS,DS}$ values and comparing them with $P^*_{LS}$. As a matter of fact, the concept of exceedance probability ($P_{f,LS,DS}$) has a stronger physical meaning if compared with both capacity margin ($Z_{LS,DS}$) and reliability index ($\beta_{LS,DS}$); this is even more intuitive considering the corresponding target values: conceptually, $P^*_{LS}$ has been defined, and $Z^*_{LS,DS}$ and $\beta^*_{LS}$ have been assessed accordingly. Further comments on Figs. 12 and 13 are omitted as these depict the results shown in Fig. 11 through a different metrology approach. Therefore, Figs. 12 and 13 are significant in terms of quantitative results and correlations with Fig. 11 and extend the field knowledge, providing reference data.

## 5. Concluding remarks

The study reported the assessment of seismic capacity and the evaluation of seismic performance of code-conforming single-story RC precast buildings, considering low to high seismicity sites in Italy. The response of the case study buildings was assessed through nonlinear multiple-stripe analyses (MSAs), according to consolidated approaches and robust models. Fragility curves were meant to express building capacities, whereas the seismic performance was assessed considering capacity margin ratios, failure probabilities, and reliability indexes. Three performance levels (PLs) were considered in the study, i.e., damage control/limitation, life safety prevention, and near collapse prevention. In particular, multiple damage criteria and damage states (DSs) were associated with each PL, considering interstory drift ratio (IDR), roof drift ratio (RDR), member end chord rotation (θ), and beam-to-column connection force ($V_{bc}$) as engineering demand parameters (EDPs); both ductile and brittle failure of beam-to-column connection were accounted for. The methodology was defined considering the latest code and literature advances, accounting for both European and US approaches. Fragility curves were assessed considering multiple methods, and capacity and performance parameters were defined and assessed through a general comprehensive approach, also providing guidance for implementation by researchers and practitioners.

The study produced a significant contribution into the field regarding both methodology and quantitative findings. The key results of the study are described in the following.

- The study provides guidance for performing a robust and consistent assessment of both seismic capacity and performance of RC precast buildings. Multiple methods were used for assessing the building fragility, as well as reasonable assumptions were provided to define the key criteria and target parameters (i.e., target reliability index).
- NPP and LSF fragility methods are confirmed to be not necessarily reliable when a reduced number of failure occurrences are observed, especially if these failures are associated with a single analysis stripe. Conversely, MLF method typically produces

relatively reliable and conservative results in the abovementioned peculiar cases. Overall, when failure is observed over multiple stripes (e.g., three or more stripes), with relatively large probabilities, the different methods tend to produce similar fragilities. Conversely, when failure only occurs for a single stripe (and the probability of failure is larger than a minimum threshold, e.g., 20%), MLF seems to supply more consistent fragilities, often being more conservative than other methods. In the case of very few failures, only over a single stripe, the definition of the best method still requires further comparison and considerations.

- IDR-based criterion associated with significant damage (i.e., $DS_{IDR,SD}$, IDR threshold equal to 2%) does not express the condition of significant structural damage and is more compatible with the yielding response of the building (i.e., $DS_{\theta y}$). A larger IDR threshold is suggested to be associated with significant structural damage, i.e., equal to 4% ($DS_{IDR,4\%}$).
- The brittle failure of the beam-to-column connection (i.e., $DS_{Vbc,b}$) is confirmed to be extremely critical since it is potentially associated with the elastic response of the building. Therefore, it should be robustly prevented by improving code and practice requirements in terms of structural details of the connection elements and devices. Conversely, the ductile failure of the connection (i.e., $DS_{Vbc,d}$) is compatible with the response associated with other severe to collapse DSs, which are consistent with the related DS severity.
- The building performance associated with damage to nonstructural elements (i.e., $DS_{IDR,NDS}$) might not be adequate for C soil type conditions, where the design prescriptions associated with relatively higher seismic demand (i.e., higher than A soil type condition) do not seem to produce a consistent and adequate increase in building capacity. A similar result is associated with significant structural damage condition, even though the authors believe that the seismic demand associated with IDR equal to 2% criterion should be revised by codes and literature, since this DS seems to be more associated with damage limitation PL.
- The building performance associated with near collapse prevention PL is adequate in all cases, even though the relatively low number of failure occurrences does not allow considering these estimations as reliable as the ones associated with other PLs.

Despite the effort of the authors in performing a robust and comprehensive assessment, the results of this study cannot be considered to be fully exhaustive and definitive, as discussed in the following. (1) The considered case studies are representative of a single structural layout, even if different geometries are investigated. Further efforts are needed to extent the validity of the work to other structural configurations. (2) The seismic assessment of RC precast buildings is performed through nonlinear dynamic analyses, following a multi-stripe approach, considering the horizontal components of the earthquake only. This choice, aiming at reducing the computational effort required for the analysis, could lead to unconservative results. Thus, a future investigation on this topic could include the effect of the vertical component of the seismic action, even though significant variations are not expected. (3) Severe to collapse DSs should be assessed further since the numerical analyses implemented in this study did not always produce an adequate number of failures.

## CRediT author statement

Gennaro Magliulo: Conceptualization, Methodology, Validation, Resources, Writing - Review & Editing, Supervision, Project administration, Funding acquisition; Danilo D'Angela: Conceptualization, Methodology, Software, Formal analysis, Investigation, Data Curation, Writing - Original Draft, Writing - Review & Editing, Visualization; Valeria Piccolo: Software, Investigation; Chiara Di Salvatore: Conceptualization, Methodology, Software, Investigation, Data Curation, Writing - Review & Editing; Nicola Caterino: Validation, Resources, Writing - Review & Editing, Funding acquisition.

## Declaration of competing interest

The authors declare that they have no known competing financial interests or personal relationships that could have appeared to influence the work reported in this paper.

## Data availability

Data will be made available on request.

## Acknowledgments

The project was funded by the Department of Civil Protection in the framework of the Re.LUIS 2022–2024 WP3 project. Authors thank Andrea Belleri, Davide Bellotti, Fabio Biondini, Bruno Dal Lago, Roberto Nascimbene, and Paolo Riva for the interesting discussions on the article topic.

## Appendix A

The column geometry and the reinforcement details resulting from the design are reported in Table A1, where $B_{col}$ is the dimension of the column (square) cross-section, $\rho$ is the longitudinal reinforcement geometric ratio, $n_l$ is the number of shear legs, $\varphi$ is the shear bar diameter, and $s$ is the shear bar spacing.

**Table A.1**
Column geometry and the reinforcement details resulting from the design.

| site | soil type | $B_{col}$ [mm] | | ρ [%] | | $n_l$-φ-s [-]-[mm]-[mm] | |
|---|---|---|---|---|---|---|---|
| | | SS | LS | SS | LS | SS | LS |
| MI | A | 750 | 850 | 1.00 | 1.00 | 5-10-110 | 3-10-55 |
| | C | 750 | 850 | 1.00 | 1.00 | 5-10-110 | 3-10-55 |
| NA | A | 750 | 850 | 1.29 | 1.25 | 3-10-65 | 4-10-75 |
| | C | 750 | 900 | 1.29 | 1.09 | 3-10-65 | 5-10-90 |
| AQ | A | 750 | 850 | 1.29 | 1.25 | 3-10-65 | 4-10-75 |
| | C | 900 | 900 | 1.34 | 1.71 | 4-10-70 | 7-8-80 |

A representative geometry of the beam-to-column connection is shown in Figure A1 (AQ site, soil type C, geometry SS), and the geometry of the dowels is reported in Table A2, where $\varphi_D$ is the dowel nominal diameter. The beam-to-column joints consisted in dowel connection systems, as this is the most common fastening system used in Europe [33]. The connection is achieved by vertical steel dowels (i.e., threaded bars) embedded in the column and passing through or inserted in designated holes in the beam. High strength mortar is injected within the holes and in some cases nuts and washers fix the top end of the dowel to the beam surface. In order to spread the vertical loads from the beams to the column, a neoprene bearing system is placed between the column and the beam.

The fundamental vibration periods ($T_1$) of the analyzed buildings are reported in Table A3, where $T_{1x}$ ($T_{1z}$) is the fundamental vibration period of the building along X (Z) direction.

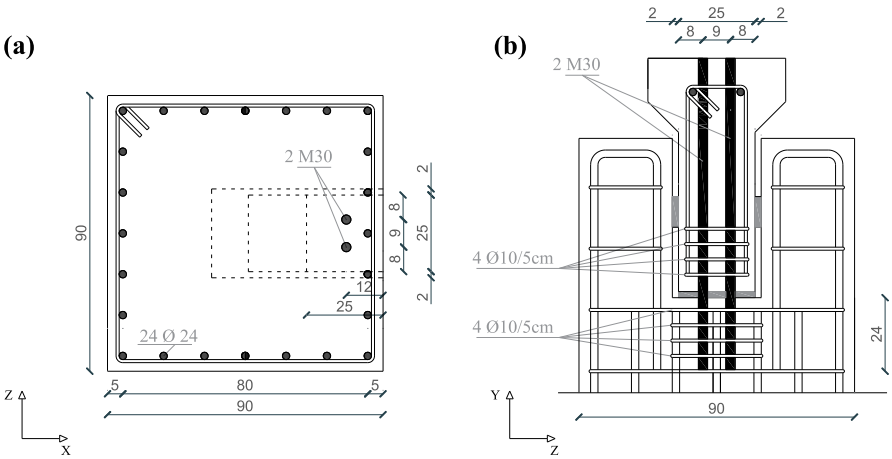


**Fig. A.1.** Beam-to-column connection details for SS building in AQ, soil C: (a) horizontal and (b) vertical section (measures in cm).

**Table A.2**
Beam-to-column connection dowels details resulting from the design.

| site | soil type | $\varphi_D$ [mm] | |
|---|---|---|---|
| | | SS | LS |
| MI | A | 18 | 20 |
| | C | 18 | 22 |
| NA | A | 20 | 27 |
| | C | 22 | 27 |
| AQ | A | 22 | 27 |
| | C | 30 | 33 |

**TableA.3**
Fundamental vibration periods of the analyzed buildings ($T_{1x}$ and $T_{1z}$) along X and Z directions.

| site | soil type | $T_{1x}$ [s] | | $T_{1z}$ [s] | |
|---|---|---|---|---|---|
| | | SS | LS | SS | LS |
| MI | A | 1.78 | 1.74 | 1.94 | 1.94 |
| | C | 1.78 | 1.74 | 1.94 | 1.94 |
| NA | A | 1.63 | 1.61 | 1.78 | 1.79 |
| | C | 1.63 | 1.52 | 1.78 | 1.70 |
| AQ | A | 1.63 | 1.61 | 1.78 | 1.79 |
| | C | 1.16 | 1.29 | 1.26 | 1.44 |

## Appendix B

Table B1 reports the failure occurrences related to all investigated cases, evaluated for all IMs. The cases associated with null occurrences are not reported.

**Table B.1**
Collapse occurrences associated with investigated case studies, computed for all IMs. $N_{EDP}$ defines the collapse occurrences due to the achievement of the capacity EDP thresholds, whereas $N_{ins}$ defines the occurrences due to instability.

| $N_{EDP}$ [−]($N_{ins}$ [−]) | | | | IM level | | | | | | | | | |
|---|---|---|---|---|---|---|---|---|---|---|---|---|---|
| IM level | site | geom. | soil type | 1 | 2 | 3 | 4 | 5 | 6 | 7 | 8 | 9 | 10 |
| DSIDR,NSD | NA | SS | A | 0 (0) | 0 (0) | 0 (0) | 0 (0) | 0 (0) | 0 (0) | 8 (0) | 22 (0) | 32 (0) | 38 (0) |
| | NA | SS | C | 0 (0) | 0 (0) | 0 (0) | 0(0) | 7(0) | 17(0) | 31(0) | 35(0) | 38(0) | 40(0) |
| | NA | LS | A | 0(0) | 0(0) | 0(0) | 0(0) | 0(0) | 0(0) | 10(0) | 21(0) | 32(0) | 38(0) |
| | NA | LS | C | 0(0) | 0(0) | 0(0) | 0(0) | 5(0) | 15(0) | 27(2) | 28(6) | 29(8) | 23(17) |
| | AQ | SS | A | 0 (0) | 0 (0) | 0 (0) | 0 (0) | 0 (0) | 0 (0) | 0 (0) | 0 (0) | 0 (0) | 27 (13) |
| | AQ | SS | C | 0 (0) | 0 (0) | 1 (0) | 6 (0) | 14 (0) | 27 (0) | 27 (0) | 39 (0) | 40 (0) | 34 (6) |
| | AQ | LS | A | 0 (0) | 0 (0) | 0 (0) | 0 (0) | 0 (0) | 0 (0) | 0 (0) | 0 (0) | 0 (0) | 26 (14) |
| | AQ | LS | C | 0 (0) | 0 (0) | 0 (0) | 8 (0) | 20 (0) | 28 (0) | 38 (0) | 40 (0) | 40 (0) | 27 (13) |
| DSIDR,SD | NA | SS | A | 0 (0) | 0 (0) | 0 (0) | 0 (0) | 0 (0) | 0 (0) | 0 (0) | 0 (0) | 1 (0) | 26 (0) |
| | NA | SS | C | 0 (0) | 0 (0) | 0 (0) | 0 (0) | 0 (0) | 0 (0) | 5 (0) | 11 (0) | 24 (0) | 35 (0) |
| | NA | LS | A | 0 (0) | 0 (0) | 0 (0) | 0 (0) | 0 (0) | 0 (0) | 0 (0) | 0 (0) | 1 (0) | 25 (0) |
| | NA | LS | C | 0 (0) | 0 (0) | 0 (0) | 0 (0) | 0 (0) | 0 (0) | 3 (0) | 12 (0) | 18 (0) | 23 (0) |
| | AQ | SS | A | 0 (0) | 0 (0) | 0 (0) | 0 (0) | 0 (0) | 0 (0) | 14 (0) | 30 (0) | 38 (0) | 24 (16) |
| | AQ | SS | C | 0 (0) | 0 (0) | 0 (0) | 0 (0) | 2 (0) | 10 (0) | 20 (0) | 28 (0) | 38 (0) | 34 (6) |
| | AQ | LS | A | 0 (0) | 0 (0) | 0 (0) | 0 (0) | 0 (0) | 0 (0) | 10 (0) | 24 (0) | 37 (0) | 27 (13) |
| | AQ | LS | C | 0 (0) | 0 (0) | 0 (0) | 0 (0) | 1 (0) | 10 (0) | 24 (0) | 34 (0) | 39 (0) | 23 (17) |
| DSIDR,4% | AQ | SS | A | 0 (0) | 0 (0) | 0 (0) | 0 (0) | 0 (0) | 0 (0) | 0 (0) | 0 (0) | 9 (0) | 26 (8) |
| | AQ | SS | C | 0 (0) | 0 (0) | 0 (0) | 0 (0) | 0 (0) | 0 (0) | 1 (0) | 6 (0) | 15 (0) | 29 (6) |
| | AQ | LS | A | 0 (0) | 0 (0) | 0 (0) | 0 (0) | 0 (0) | 0 (0) | 0 (0) | 0 (0) | 9 (0) | 21 (13) |
| | AQ | LS | C | 0 (0) | 0 (0) | 0 (0) | 0 (0) | 0 (0) | 0 (0) | 3 (0) | 6 (0) | 23 (0) | 23 (17) |
| DSθu | AQ | SS | A | 0 (0) | 0 (0) | 0 (0) | 0 (0) | 0 (0) | 0 (0) | 0 (0) | 0 (0) | 0 (0) | 14 (0) |
| | AQ | SS | C | 0 (0) | 0 (0) | 0 (0) | 0 (0) | 0 (0) | 0 (0) | 0 (0) | 0 (0) | 0 (0) | 4 (0) |
| | AQ | LS | A | 0 (0) | 0 (0) | 0 (0) | 0 (0) | 0 (0) | 0 (0) | 0 (0) | 0 (0) | 0 (0) | 14 (0) |
| | AQ | LS | C | 0 (0) | 0 (0) | 0 (0) | 0 (0) | 0 (0) | 0 (0) | 0 (0) | 0 (0) | 0 (0) | 14 (0) |
| DSVbc,b | MI | SS | A | 0 (0) | 0 (0) | 0 (0) | 0 (0) | 0 (0) | 0 (0) | 0 (0) | 0 (0) | 0 (0) | 8 (0) |
| | MI | SS | C | 0 (0) | 0 (0) | 0 (0) | 0 (0) | 0 (0) | 0 (0) | 0 (0) | 0 (0) | 3 (0) | 18 (0) |
| | MI | LS | A | 0 (0) | 0 (0) | 0 (0) | 0 (0) | 0 (0) | 0 (0) | 0 (0) | 6 (0) | 15 (0) | 19 (0) |
| | MI | LS | C | 0 (0) | 0 (0) | 0 (0) | 0 (0) | 0 (0) | 0 (0) | 2 (0) | 9 (0) | 17 (0) | 20 (0) |
| | NA | SS | A | 0 (0) | 0 (0) | 0 (0) | 1 (0) | 6 (0) | 17 (0) | 20 (0) | 19 (0) | 35 (0) | 39 (0) |
| | NA | SS | C | 0 (0) | 0 (0) | 0 (0) | 7 (0) | 12 (0) | 19 (0) | 28 (0) | 36 (0) | 35 (0) | 38 (6) |
| | NA | LS | A | 0 (0) | 0 (0) | 0 (0) | 0 (0) | 0 (0) | 3 (0) | 13 (0) | 25 (0) | 33 (0) | 39 (0) |
| | NA | LS | C | 0 (0) | 0 (0) | 0 (0) | 4 (0) | 7 (0) | 24 (0) | 33 (0) | 37 (0) | 36 (0) | 40 (0) |
| | AQ | SS | A | 0 (0) | 0 (0) | 0 (0) | 4 (0) | 14 (0) | 20 (0) | 34 (0) | 40 (0) | 40 (0) | 26 (14) |
| | AQ | SS | C | 0 (0) | 0 (0) | 2 (0) | 10 (0) | 23 (0) | 29 (0) | 40 (0) | 39 (0) | 40 (0) | 34 (6) |
| | AQ | LS | A | 0 (0) | 0 (0) | 0 (0) | 1 (0) | 6 (0) | 23 (0) | 36 (0) | 40 (0) | 40 (0) | 26 (14) |
| | AQ | LS | C | 0 (0) | 0 (0) | 2 (0) | 13 (0) | 24 (0) | 37 (0) | 40 (0) | 40 (0) | 40 (0) | 22 (18) |
| DSVbc,d | NA | SS | A | 0 (0) | 0 (0) | 0 (0) | 0 (0) | 0 (0) | 0 (0) | 0 (0) | 0 (0) | 0 (0) | 26 (0) |
| | NA | LS | C | 0 (0) | 0 (0) | 0 (0) | 0 (0) | 5 (0) | 15 (0) | 27 (2) | 28 (6) | 29 (8) | 23 (17) |
| | AQ | SS | A | 0 (0) | 0 (0) | 0 (0) | 0 (0) | 0 (0) | 0 (0) | 0 (0) | 0 (0) | 0 (0) | 1 (14) |
| | AQ | SS | C | 0 (0) | 0 (0) | 0 (0) | 0 (0) | 0 (0) | 0 (0) | 0 (0) | 0 (0) | 0 (0) | 0 (6) |
| | AQ | LS | A | 0 (0) | 0 (0) | 0 (0) | 0 (0) | 0 (0) | 0 (0) | 0 (0) | 0 (0) | 0 (0) | 0 (14) |
| | AQ | LS | C | 0 (0) | 0 (0) | 0 (0) | 0 (0) | 0 (0) | 0 (0) | 0 (0) | 0 (0) | 0 (0) | 0 (18) |
| DSRDRu | AQ | SS | A | 0 (0) | 0 (0) | 0 (0) | 0 (0) | 0 (0) | 0 (0) | 0 (0) | 0 (0) | 0 (0) | 1 (14) |
| | AQ | SS | C | 0 (0) | 0 (0) | 0 (0) | 0 (0) | 0 (0) | 0 (0) | 0 (0) | 0 (0) | 0 (0) | 0 (6) |
| | AQ | LS | A | 0 (0) | 0 (0) | 0 (0) | 0 (0) | 0 (0) | 0 (0) | 0 (0) | 0 (0) | 0 (0) | 0 (13) |
| | AQ | LS | C | 0 (0) | 0 (0) | 0 (0) | 0 (0) | 0 (0) | 0 (0) | 0 (0) | 0 (0) | 0 (0) | 0 (6) |

## References

[1] M. Ercolino, G. Magliulo, G. Manfredi, Failure of a precast RC building due to Emilia-Romagna earthquakes, Eng. Struct. 118 (2016) 262–273, https://doi.org/10.1016/j.engstruct.2016.03.054.
[2] L. Liberatore, L. Sorrentino, D. Liberatore, L.D. Decanini, Failure of industrial structures induced by the Emilia (Italy) 2012 earthquakes, Eng. Fail. Anal. 34 (2013) 629–647, https://doi.org/10.1016/j.engfailanal.2013.02.009.
[3] G. Magliulo, M. Ercolino, C. Petrone, O. Coppola, G. Manfredi, The emilia earthquake: seismic performance of precast reinforced concrete buildings, Earthq. Spectra 30 (2014) 891–912, https://doi.org/10.1193/091012EQS285M.
[4] M. Savoia, N. Buratti, L. Vincenzi, Damage and collapses in industrial precast buildings after the 2012 Emilia earthquake, Eng. Struct. 137 (2017) 162–180, https://doi.org/10.1016/j.engstruct.2017.01.059.
[5] M. Saatcioglu, D. Mitchell, R. Tinawi, N.J. Gardner, A.G. Gillies, A. Ghobarah, D.L. Anderson, D. Lau, The August 17, 1999, Kocaeli (Turkey) earthquake — damage to structures, Can. J. Civ. Eng. 28 (2001) 715–737, https://doi.org/10.1139/cjce-28-4-715.

[6] G. Toniolo, A. Colombo, Precast concrete structures: the lessons learned from the L'Aquila earthquake, Struct. Concr. 13 (2012) 73–83, https://doi.org/10.1002/suco.201100052.
[7] M. Posada, S. Wood, Seismic performance of precast industrial buildings in Turkey, in: Proc 7th US Natl. Conf, . Earthq. Eng., EERI, Boston, MA, 2002.
[8] S. Ozden, E. Akpinar, H. Erdogan, H.M. Atalay, Performance of precast concrete structures in October 2011 Van earthquake, Turkey, Mag. Concr. Res. 66 (2014) 543–552, https://doi.org/10.1680/macr.13.00097.
[9] F. Clementi, A. Scalbi, S. Lenci, Seismic performance of precast reinforced concrete buildings with dowel pin connections, J. Build. Eng. 7 (2016) 224–238, https://doi.org/10.1016/j.jobe.2016.06.013.
[10] M. Cimmino, G. Magliulo, G. Manfredi, Seismic collapse assessment of new European single-story RC precast buildings with weak connections, Bull. Earthq. Eng. (2020), https://doi.org/10.1007/s10518-020-00952-7.
[11] J. Zhang, C. Li, X. Rong, X. Zhang, Y. Li, Experimental study on the seismic performance of steel–concrete beam–column connections for prefabricated concrete frames, J. Build. Eng. 43 (2021), 103236, https://doi.org/10.1016/j.jobe.2021.103236.
[12] B. Zoubek, M. Fischinger, T. Isaković, Cyclic response of hammer-head strap cladding-to-structure connections used in RC precast building, Eng. Struct. 119 (2016) 135–148, https://doi.org/10.1016/j.engstruct.2016.04.002.
[13] M. Ercolino, G. Magliulo, G. Manfredi, Seismic performance of single-story precast buildings: effect of cladding panels, J. Struct. Eng. 144 (2018), 04018134, https://doi.org/10.1061/(ASCE)ST.1943-541X.0002114.
[14] B. Zoubek, A. Babič, M. Dolšek, M. Fischinger, T. Isaković, Recent advances in the research of the seismic response of RC precast buildings at the university of ljubljana, Front.Built.Environ. 7 (2021), 630952, https://doi.org/10.3389/fbuil.2021.630952.
[15] M. Ercolino, D. Bellotti, G. Magliulo, R. Nascimbene, Vulnerability analysis of industrial RC precast buildings designed according to modern seismic codes, Eng. Struct. 158 (2018) 67–78, https://doi.org/10.1016/j.engstruct.2017.12.005.
[16] RINTC Workgroup, Results of the 2015-2017 Implicit Seismic Risk of Code-Conforming Structures in Italy (RINTC) Project, Rete dei Laboratori Universitari di Ingegneria Sismica (ReLUIS), Naples, 2018.
[17] C. Casotto, V. Silva, H. Crowley, R. Nascimbene, R. Pinho, Seismic fragility of Italian RC precast industrial structures, Eng. Struct. 94 (2015) 122–136, https://doi.org/10.1016/j.engstruct.2015.02.034.
[18] D. Beilic, C. Casotto, R. Nascimbene, D. Cicola, D. Rodrigues, Seismic fragility curves of single storey RC precast structures by comparing different Italian codes, Earthq, Struct 12 (2017) 359–374, https://doi.org/10.12989/EAS.2017.12.3.359.
[19] A. Babič, M. Dolšek, Seismic fragility functions of industrial precast building classes, Eng. Struct. 118 (2016) 357–370, https://doi.org/10.1016/j.engstruct.2016.03.069.
[20] G. Magliulo, G. Fabbrocino, G. Manfredi, Seismic assessment of existing precast industrial buildings using static and dynamic nonlinear analyses, Eng. Struct. 30 (2008) 2580–2588, https://doi.org/10.1016/j.engstruct.2008.02.003.
[21] C. Demartino, I. Vanzi, G. Monti, C. Sulpizio, Precast industrial buildings in Southern Europe: loss of support at frictional beam-to-column connections under seismic actions, Bull. Earthq. Eng. 16 (2018) 259–294, https://doi.org/10.1007/s10518-017-0196-5.
[22] Federal Emergency Management Agency (FEMA), Quantification of Building Seismic Performance Factors, 2009. Report No. P695., Washington D.C., USA.
[23] I. Iervolino, M. Dolce, Foreword to the special issue for the RINTC (the implicit seismic risk of code-conforming structures) project, J. Earthq. Eng. 22 (2018) 1–4, https://doi.org/10.1080/13632469.2018.1543697.
[24] I. Iervolino, R. Baraschino, A. Belleri, D. Cardone, G. Della Corte, P. Franchin, S. Lagomarsino, G. Magliulo, A. Marchi, A. Penna, L.R.S. Viggiani, A. Zona, Seismic fragility of Italian code-conforming buildings by multi-stripe dynamic analysis of three-dimensional structural models, J. Earthq. Eng. (2023) 1–34, https://doi.org/10.1080/13632469.2023.2167889.
[25] I. Iervolino, A. Spillatura, P. Bazzurro, Seismic reliability of code-conforming Italian buildings, J. Earthq. Eng. 22 (2018) 5–27, https://doi.org/10.1080/13632469.2018.1540372.
[26] Consiglio Superiore dei Lavori Pubblici (CS.LL.PP.), D.M. del 14/01/2008 – "Norme tecniche per le Costruzioni 2008", NTC, 2008, p. 2008 (in Italian).
[27] CEN, EN 1998–3, Eurocode 8: Design of Structures for Earthquake Resistance - Part 3: Assessment and Retrofitting of Buildings, 2005.
[28] CEN, EN 1992–1-1, Eurocode 2: Design of Concrete Structures - Part 1-1: General Rules and Rules for Buildings, 2004.
[29] Consiglio Superiore dei Lavori Pubblici (CS.LL.PP.), D.M. del 17/01/2018 – "Aggiornamento delle Norme tecniche per le Costruzioni 2018" NTC 2018 (in Italian), 2018.
[30] RINTC Workgroup, Results of the 2015-2017 Implicit Seismic Risk of Code-Conforming Structures in Italy (RINTC) Project, Rete dei Laboratori Universitari di Ingegneria Sismica (ReLUIS), Naples, 2018.
[31] P. Ricci, V. Manfredi, F. Noto, M. Terrenzi, C. Petrone, F. Celano, M.T. De Risi, G. Camata, P. Franchin, G. Magliulo, A. Masi, F. Mollaioli, E. Spacone, G. M. Verderame, Modeling and seismic response analysis of Italian code-conforming reinforced concrete buildings, J. Earthq. Eng. 22 (2018) 105–139, https://doi.org/10.1080/13632469.2018.1527733.
[32] CNR, CNR 10025/84, Istruzioni per il progetto, l'esecuzione ed il controllo delle strutture prefabbricate in conglomerato cementizio e per le strutture construite con sistemi industrializzati (in Italian), Bollettino Ufficiale del CNR, 1985.
[33] G. Magliulo, D. Bellotti, M. Cimmino, R. Nascimbene, Modeling and seismic response analysis of RC precast Italian code-conforming buildings, J. Earthq. Eng. 22 (2018) 140–167, https://doi.org/10.1080/13632469.2018.1531093.
[34] Applied Technology Council (ATC), Seismic Performance Assessment of Buildings FEMA P-58-1, 2018. Washington, DC.
[35] C. Meletti, V. Montaldo, Stime di pericolosità sismica per diverse probabilità di superamento in 50 anni: valori di ag, Progetto DPC-INGV S1, Deliverable D2 (in Italian), http://esse1.mi.ingv.it/d2.html, 2007.
[36] D. D'Angela, G. Magliulo, E. Cosenza, Characterization of local and global capacity criteria for collapse assessment of code-conforming RC buildings, Bull. Earthq. Eng. (2021), https://doi.org/10.1007/s10518-021-01115-y.
[37] A. Belleri, M. Torquati, A. Marini, P. Riva, Horizontal cladding panels: in-plane seismic performance in precast concrete buildings, Bull. Earthq. Eng. 14 (2016) 1103–1129, https://doi.org/10.1007/s10518-015-9861-8.
[38] M.N. Fardis, D. Biskinis, Deformation capacity of RC members, as controlled by flexure or shear, in: Otani Symp, 2003, pp. 511–530.
[39] M. Fischinger, M. Kramar, T. Isaković, Cyclic response of slender RC columns typical of precast industrial buildings, Bull. Earthq. Eng. 6 (2008) 519–534, https://doi.org/10.1007/s10518-008-9064-7.
[40] CEN, draft of new EN 1998–1-2, Eurocode 8: Design of Structures for Earthquake Resistance - Part 1-2: Rules for New Buildings, 2020.
[41] C.B. Haselton, G.G. Deierlein, The john A. Blume earthquake engineering center, in: Assessing Seismic Collapse Safety of Modern Reinforced Concrete Moment Frame Buildings, Department of Civil and Environmental engineering. Stanford University, Stanford CA, 2007.
[42] C.B. Haselton, A.B. Liel, S. Taylor-Lange, G.G. Deierlein, PEER Report No. 2007/03, Beam-column Element Model Calibrated for Predicting Flexural Response Leading to Global Collapse of RC Frame Buildings, Pacific Earthquake Engineering Research Center, University of California, Berkeley, CA, 2008.
[43] T.P. Vintzēleou, E.N. Tassios, Behavior of dowels under cyclic deformations, ACI Struct. J. 84 (1987), https://doi.org/10.14359/2749.
[44] B. Zoubek, M. Fischinger, T. Isakovic, Estimation of the cyclic capacity of beam-to-column dowel connections in precast industrial buildings, Bull. Earthq. Eng. 13 (2015) 2145–2168, https://doi.org/10.1007/s10518-014-9711-0.
[45] I.N. Psycharis, H.P. Mouzakis, Shear resistance of pinned connections of precast members to monotonic and cyclic loading, Eng. Struct. 41 (2012) 413–427, https://doi.org/10.1016/j.engstruct.2012.03.051.
[46] European Commission, Joint Research Centre. Institute for the Protection and the Security of the Citizen, Design Guidelines for Connections of Precast Structures under Seismic Actions, Publications Office, LU, 2012. https://data.europa.eu/doi/10.2777/37605. (Accessed 11 March 2021).
[47] EOTA, TR029, Design of Bonded Anchors, 2007.
[48] EOTA, TR045, Design of Metal Anchors for Use in Concrete under Seismic Actions, 2013.
[49] E.N. Vintzēleou, T.P. Tassios, Mathematical models for dowel action under monotonic and cyclic conditions, Mag. Concr. Res. 38 (1986) 13–22, https://doi.org/10.1680/macr.1986.38.134.13.

[50] G. Camata, F. Celano, M.T. De Risi, P. Franchin, G. Magliulo, V. Manfredi, A. Masi, F. Mollaioli, F. Noto, P. Ricci, E. Spacone, M. Terrenzi, G. Verderame, Rintc project: nonlinear dynamic analyses of Italian code-conforming reinforced concrete buildings for risk of collapse assessment, in: Proc. 6th Int. Conf. Comput. Methods Struct. Dyn. Earthq. Eng. COMPDYN 2015, Institute of Structural Analysis and Antiseismic Research School of Civil Engineering National Technical University of Athens (NTUA) Greece, Rhodes Island, Greece, 2017, pp. 1474–1485, https://doi.org/10.7712/120117.5507.17050.
[51] N. Luco, B.R. Ellingwood, R.O. Hamburger, J.D. Hooper, J.K. Kimball, C.A. Kircher, Risk-targeted versus current seismic design maps for the conterminous United States, in: SEAOC 2007 Conv, Proc., 2007.
[52] American Society of Civil Engineers (Ed.), ASCE 7-16. Minimum Design Loads for Buildings and Other Structures, American Society of Civil Engineers : Structural Engineering Institute, Reston, Va, 2017.
[53] F. McKenna, G.L. Fenves, M.H. Scott, OpenSees: Open System for Earthquake Engineering Simulation. Pacific Earthquake Engineering Research Center, University of California, Berkeley, CA, 2000. Available at: http://opensees.berkeley.edu.
[54] G. Magliulo, M. Ercolino, G. Manfredi, Influence of cladding panels on the first period of one-story precast buildings, Bull. Earthq. Eng. 13 (2015) 1531–1555, https://doi.org/10.1007/s10518-014-9657-2.
[55] F. Gusella, Effect of the plastic rotation randomness on the moment redistribution in reinforced concrete structures, Eng. Struct. 252 (2022), 113652, https://doi.org/10.1016/j.engstruct.2021.113652.
[56] L.F. Ibarra, H. Krawinkler, Global Collapse of Frame Structures under Seismic Excitations, the John A. Blume Earthquake Engineering Center, Department of Civil and Environmental engineering. Stanford University, Stanford CA, 2005.
[57] L.F. Ibarra, R.A. Medina, H. Krawinkler, Hysteretic models that incorporate strength and stiffness deterioration, Earthq. Eng. Struct. Dynam. 34 (2005) 1489–1511, https://doi.org/10.1002/eqe.495.
[58] T.L. Karavasilis, J.M. Ricles, R. Sause, Implementation of Deterioration Elements in OpenSEES for Collapse Simulations, ATLSS Engineering Research Center, 2009.
[59] J.B. Mander, M.J.N. Priestley, R. Park, Theoretical stress-strain model for confined concrete, J. Struct. Eng. 114 (1988) 1804–1826, https://doi.org/10.1061/(ASCE)0733-9445(1988)114:8(1804).
[60] M. Ercolino, C. Petrone, G. Magliulo, G. Manfredi, Seismic design of single-story precast structures for $P$ -Δ effects, ACI Struct. J. 115 (2018), https://doi.org/10.14359/51701915.
[61] F. Jalayer, Direct Probabilistic Seismic Analysis: Implementing Nonlinear Dynamic Assessment, PhD Thesis, Department of Civil and Environmental Engineering, Stanford University, 2003.
[62] F. Scozzese, E. Tubaldi, A. Dall'Asta, Assessment of the effectiveness of Multiple-Stripe Analysis by using a stochastic earthquake input model, Bull. Earthq. Eng. 18 (2020) 3167–3203, https://doi.org/10.1007/s10518-020-00815-1.
[63] I. Iervolino, A. Spillatura, P. Bazzurro, Rintc project - assessing the (implicit) seismic risk of code-conforming structures in Italy, in: Proc. 6th Int. Conf. Comput. Methods Struct. Dyn. Earthq. Eng. COMPDYN 2015, Institute of Structural Analysis and Antiseismic Research School of Civil Engineering National Technical University of Athens (NTUA) Greece, Rhodes Island, Greece, 2017, pp. 1545–1557, https://doi.org/10.7712/120117.5512.17282.
[64] T. Lin, C.B. Haselton, J.W. Baker, Conditional spectrum-based ground motion selection. Part I: hazard consistency for risk-based assessments, Earthq. Eng. Struct. Dynam. 42 (2013) 1847–1865, https://doi.org/10.1002/eqe.2301.
[65] N. Jayaram, T. Lin, J.W. Baker, A computationally efficient ground-motion selection algorithm for matching a target response spectrum mean and variance, Earthq. Spectra 27 (2011) 797–815, https://doi.org/10.1193/1.3608002.
[66] K. Porter, A beginner's guide to fragility, vulnerability, and risk. http://spot.colorado.edu/~porterka/Porter-beginnersguide.pdf, 2019.
[67] R. Baraschino, G. Baltzopoulos, I. Iervolino, R2R-Eu, Software for fragility fitting and evaluation of estimation uncertainty in seismic risk analysis, Soil Dynam. Earthq. Eng. 132 (2020), 106093, https://doi.org/10.1016/j.soildyn.2020.106093.
[68] I. Iervolino, Assessing uncertainty in estimation of seismic response for PBEE, Earthq. Eng. Struct. Dynam. 46 (2017) 1711–1723, https://doi.org/10.1002/eqe.2883.
[69] N. Shome, C.A. Cornell, Structural seismic demand analysis: consideration of "collapse, in: Proc. 8th ACSE Spec. Conf. Probabilistic Mech. Struct. Reliab, 2000. South Bend, Indiana.
[70] J.W. Baker, Efficient analytical fragility function fitting using dynamic structural analysis, Earthq. Spectra 31 (2015) 579–599, https://doi.org/10.1193/021113EQS025M.
[71] C.A. Cornell, J.R. Benjamin, Probability, Statistics and Decision for Civil Engineers, McGraw-Hill, New York, NY, 1970.
[72] N.R. Draper, H. Smith, Applied Regression Analysis, third ed., John Wiley & Sons, New York, NY, 1998.
[73] C.B. Haselton, A.B. Liel, G.G. Deierlein, B.S. Dean, J.H. Chou, Seismic collapse safety of reinforced concrete buildings. I: assessment of ductile moment frames, J. Struct. Eng. 137 (2011) 481–491, https://doi.org/10.1061/(ASCE)ST.1943-541X.0000318.
[74] L. Xuchuan, M. Kato, L. Zhang, M. Nakashima, Quantitative investigation on collapse margin of steel high-rise buildings subjected to extremely severe earthquakes, Earthq. Eng. Eng. Vib. 17 (2018) 445–457, https://doi.org/10.1007/s11803-018-0454-9.
[75] T. Becker, S. Furukawa, S.A. Mahin, M. Nakashima, Comparison of US and Japanese codes and practices for seismically isolated buildings, in: Proc. 2010 Struct. Congr. ASCE, ASCE, 2010, pp. 2330–2338, https://doi.org/10.1061/41130(369)211.
[76] C.B. Haselton, J.W. Baker, J.P. Stewart, A.S. Whittaker, N. Luco, A. Fry, R.O. Hamburger, R.B. Zimmerman, J.D. Hooper, F.A. Charney, R.G. Pekelnicky, Response history analysis for the design of new buildings in the NEHRP provisions and ASCE/SEI 7 standard: Part I - overview and specification of ground motions, Earthq. Spectra 33 (2017) 373–395, https://doi.org/10.1193/032114EQS039M.
[77] P. Fajfar, Analysis in seismic provisions for buildings: past, present and future: the fifth Prof. Nicholas Ambraseys lecture, Bull. Earthq. Eng. 16 (2018) 2567–2608, https://doi.org/10.1007/s10518-017-0290-8.
[78] J.W. Baker, C.A. Cornell, Spectral shape, epsilon and record selection, Earthq. Eng. Struct. Dynam. 35 (2006) 1077–1095, https://doi.org/10.1002/eqe.571.
[79] Y. Zhang, Z. He, Acceptable values of collapse margin ratio with different confidence levels, Struct. Saf. 84 (2020), 101938, https://doi.org/10.1016/j.strusafe.2020.101938.
[80] M. Kramar, T. Isaković, M. Fischinger, Seismic collapse risk of precast industrial buildings with strong connections, Earthq. Eng. Struct. Dynam. (2009) 847–868, https://doi.org/10.1002/eqe.970.
[81] M. Deyanova, S. Pampanin, R. Nascimbene, Assessment of single-storey precast concrete industrial buildings with hinged beam-column connections with and without dowels, in: Proc. Second Eur. Conf. Earthq. Eng. Seismol, EAEE, Istanbul, 2014, pp. 1–14.